



Structure-activity relationship study of THZ531 derivatives enables the discovery of BSJ-01-175 as a dual CDK12/13 covalent inhibitor with efficacy in Ewing sarcoma



Baishan Jiang^{a, b, 1}, Jie Jiang^{a, b, 1}, Ines H. Kaltheuner^{c, 1}, Amanda Balboni Iniguez^{d, e}, Kanchan Anand^c, Fleur M. Ferguson^{a, b}, Scott B. Ficarro^{a, f}, Bo Kyung Alex Seong^{d, e}, Ann Katrin Greifenberg^c, Sofia Dust^c, Nicholas P. Kwiatkowski^{a, b}, Jarrod A. Marto^{a, f}, Kimberly Stegmaier^{d, e}, Tinghu Zhang^{a, b, **}, Matthias Geyer^{c, ***}, Nathanael S. Gray^{a, b, *}

^a Department of Cancer Biology, Dana-Farber Cancer Institute, Harvard Medical School, Boston, MA, 02115, USA

^b Department of Biological Chemistry and Molecular Pharmacology, Harvard Medical School, Boston, MA, 02115, USA

^c Institute of Structural Biology, University of Bonn, Venusberg-Campus 1, 53127, Bonn, Germany

^d Department of Pediatric Oncology, Dana-Farber Cancer Institute, Harvard Medical School, Boston, MA, 02115, USA

^e The Broad Institute, Cambridge, MA, 02142, USA

^f Blais Proteomics Center, Dana-Farber Cancer Institute, Harvard Medical School, Boston, MA, 02215, USA

ARTICLE INFO

Article history:

Received 7 February 2021

Received in revised form

13 April 2021

Accepted 14 April 2021

Available online 20 April 2021

Keywords:

CDK12/13

Covalent inhibitor

Structure-activity relationship

ABSTRACT

Development of inhibitors targeting CDK12/13 is of increasing interest as a potential therapy for cancers as these compounds inhibit transcription of DNA damage response (DDR) genes. We previously described THZ531, a covalent inhibitor with selectivity for CDK12/13. In order to elucidate structure-activity relationship (SAR), we have undertaken a medicinal chemistry campaign and established a focused library of THZ531 analogs. Among these analogs, BSJ-01-175 demonstrates exquisite selectivity, potent inhibition of RNA polymerase II phosphorylation, and downregulation of CDK12-targeted genes in cancer cells. A 3.0 Å co-crystal structure with CDK12/CycK provides a structural rationale for selective targeting of Cys1039 located in a C-terminal extension from the kinase domain. With moderate pharmacokinetic properties, BSJ-01-175 exhibits efficacy against an Ewing sarcoma tumor growth in a patient-derived xenograft (PDX) mouse model following 10 mg/kg once a day, intraperitoneal administration. Taken together, BSJ-01-175 represents the first selective CDK12/13 covalent inhibitor with *in vivo* efficacy reported to date.

© 2021 Elsevier Masson SAS. All rights reserved.

1. Introduction

The human genome encodes 21 cyclin-dependent kinases (CDKs), serine/threonine kinases that require cyclin binding for activity [1,2]. Based on the nature of cellular processes they regulate, CDKs are divided into two subfamilies: cell cycle CDKs (CDK1-6, 11 and CDK14-18) and transcriptional CDKs (tCDKs; CDK7-13, 19

and 20) [3,4]. Although cell cycle CDKs were the first to be discovered and studied, tCDKs have been of increasing interest given their role as regulators of gene transcription, either as the kinases of RNA polymerase (pol) II protein complex or as part of transcriptional mediator [5,6]. CDK12 and its close homolog CDK13, both activated through cyclin K binding, were recently identified as kinases responsible for RNA pol II Ser2 phosphorylation which is required to sustain transcriptional elongation [7–10]. Although genetic deletion of either *CDK12* or *CDK13* leads to a down-regulation of more than 1000 overlapping genes [10], genes that regulate protein translation are more sensitive to *CDK13* deletion, while DNA-damage responsive (DDR) genes are more sensitive to *CDK12* deletion. This suggested an opportunity for combining CDK12-targeting inhibitors with inhibitors of PARP, a single-strand break DNA repair protein, to achieve an enhanced cancer cell killing

* Corresponding author. Department of Cancer Biology, Dana-Farber Cancer Institute, Harvard Medical School, Boston, MA, 02115, USA.

** Corresponding author. Department of Biological Chemistry and Molecular Pharmacology, Harvard Medical School, Boston, MA, 02115, USA.

*** Corresponding author.

E-mail address: nathanael_gray@dfci.harvard.edu (N.S. Gray).

¹ These three authors contributed equally to this work.

effect [11–15]. For example, a combination treatment of Olaparib, a PARP inhibitor, and Dinaciclib, a clinical pan-CDK inhibitor, synergistically suppress tumor growth in an ovarian patient-derived xenograft (PDX) model [16]. A similar synergistic effect was observed in a mouse model of Ewing sarcoma [17]. These initial proof-of-concept results intensified our interest in developing small molecule inhibitors for CDK12.

We have recently described an initial CDK12/13-selective covalent inhibitor THZ531, which was developed starting from THZ1, a CDK7/CDK12/13 covalent inhibitor (Fig. 1) [18,19]. We also established that CDK12/13 selectivity of THZ531 over CDK7 is structurally derived from 3-aminopiperidine moiety, which discriminates the targeted cysteine Cys1039 on CDK12 (or Cys1017 on CDK13) from Cys312 on CDK7. To further understand its structural-activity relationships (SAR), we designed and synthesized a focused library of THZ531 analogs with 3-aminopiperidine scaffold or its variation. Here, we present the results of these efforts, including a structure-activity relationship (SAR) and a selectivity/potency improvement for this series of compounds.

2. Results and discussion

2.1. Chemistry

The synthesis of **10a–10h** is illustrated in Scheme 1. The commercially available (1-(phenylsulfonyl)-1H-indol-3-yl) boronic acid was coupled with 2,4-pyrimidine using a Suzuki reaction, followed by S_N2 reaction with N-Boc protected 3-aminopyrrolidine or its analogs: 3-aminopyrrolidine and 3-aminoazepan. The removal of Boc group allowed intermediate **5** to react with 4-nitrobenzoic acid or 5-nitropicolinic acid. Subsequent reduction of nitro group (**7**) with SnCl_2 in acidic conditions led to compound **8**, which then reacted with either acryloyl chloride or (*E*)-4-bromobut-2-enoyl chloride followed by dimethyl amine to replace the bromide. The final product **10** was obtained after deprotection of phenylsulfonyl group from **9**.

Scheme 2 described the synthesis for compounds **15a–15h**. The common intermediate **5** was converted to a series of analogs **12** by a nucleophilic substitution with 1-fluoro-4-nitrobenzene or 2-fluoro-5-nitropyridine or related derivatives. The nitro group was reduced to free amino group, which was then coupled with acrylamide or with (*E*)-4-bromobut-2-enoyl chloride. Compound **14** was then heated under basic conditions to deprotect the phenylsulfonyl group and afford the final product **15**.

The synthesis of **22a–22e** is depicted in Scheme 3. Substitution of 1-fluoro-4-nitrobenzene with 3-aminocyclohexan-1-ol afforded **18**, which was coupled with **3a** at elevated temperatures to provide **19**. Subsequent reduction resulted in free amine compound **20**, which was then coupled with acrylamide or (*E*)-4-bromobut-2-enoyl chloride and afforded **21**. The final product **22** was obtained upon deprotection in the presence of 1 M NaOH solution.

2.2. SAR analysis leads to the identification of BSJ-01-175

All compounds were tested for their CDK12/13 inhibitory activity using a radiometric kinase assay that measures

phosphorylation of His-*c*-Myc (aa 17–167) as a substrate of recombinant CDK12 and 13 proteins. The commercial kinase assays from Invitrogen, ADAPTA or Z'LYTE, were chosen to measure the biochemical inhibitory IC_{50} values for CDK2/CycA, CDK7/CycH and CDK9/CycT1 using a fixed-time point format.

The initial THZ531 modifications included replacing the chloride with bromide, cyclopropane and trifluoromethyl. As shown in Table 1, **10b** (bromide derivative) maintained nearly equal potency as THZ531 on all CDKs tested, whereas **10c** and **10d** (cyclopropane and trifluoromethyl derivatives, respectively) exhibited a dramatic loss of activity, indicating the potential for a steric clash between these bulky groups and Phe813 on CDK12 or Phe791 on CDK13, respectively. Next, changing the size of the central saturated ring of THZ531 with 3-aminopyrrolidine (**10e**) and 3-aminoazepan (**10f**) led to a divergent activity shift. The smaller pyrrolidine group enhanced the activities on CDK2/7/9/12/13, whereas bulkier 3-aminoazepan abrogated the activities on CDK12/13. We therefore fixed 3-aminopiperidine as the central ring and introduced a pyridine ring to compound **10g**, which displayed a slight increase of IC_{50} relative to THZ531. Interestingly, removing methylene dimethyl amine (DMA) from compound **10g** restored the inhibitory activity on CDK12/13 by compound **10h**, likely due to less steric interactions.

Further modifications were focused on decreasing the size of the compound by removing carbonyl group and conjugated piperidine to the extended aromatic ring which contains the covalent warhead. As shown in Table 2, compound **15a** has 3–5-fold increase of activity on CDK2, CDK7 and CDK12/13, while almost no change on CDK9. However, this increased activity on CDK2 and CDK7 was mitigated once the DMA group was removed, as shown by compound **15b** which retained the activity on CDK12/13 while decreasing activity on CDK2, 7 and 9. The same trend was observed with compounds **15c** and **15d**, which are pyridine versions of **15a** and **15b**, respectively, suggesting that removal of the DMA group improves selectivity for CDK12/13 over CDK2 and 7. Next, we introduced small substitution groups, such as F, Me or OMe to either 3- or 6-position of the phenyl ring (compounds **15e–15h**). The mono-substitution with F or Me on either the 3 or 6 position was well tolerated by CDK12/13 (**15e** and **15f**). The bis-substitution with F and Me resulted in a compound that unexpectedly gained some activity on CDK2, although it still maintained activity for CDK12/13 (**15g**). Installing an OMe group at the 3-position to replace F indeed abrogates this gained activity on CDK2 (**15h**). Additionally, compound **15h** exhibited differential activity on CDK12 and CDK13, with IC_{50} of 293.2 nM and 4385 nM, respectively. Therefore, **15h** provides a potential lead for developing selective inhibitors for CDK12 over CDK13.

The results we obtained with derivatives featuring DMA group in both the **10** and **15** series suggested that either an amide bond or the direct connection between piperidine and phenyl resulted in a rigidity of the molecule and thus restrained the acrylamide warhead. To explore this issue further, we introduced a more flexible ether linker as a strategy to mitigate DMA's influence, and thus compound BSJ-01-175 (**22a**) and its DMA-free version **22b** were synthesized. As expected, both compounds inhibited CDK12 with the same biochemical IC_{50} of 155 nM, a 3-fold decrease

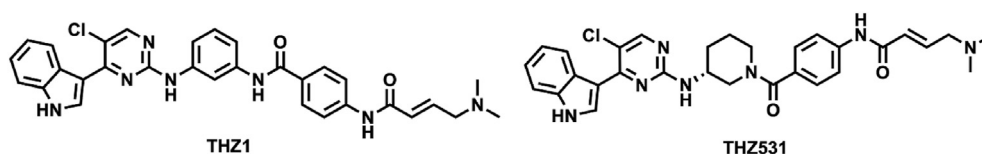
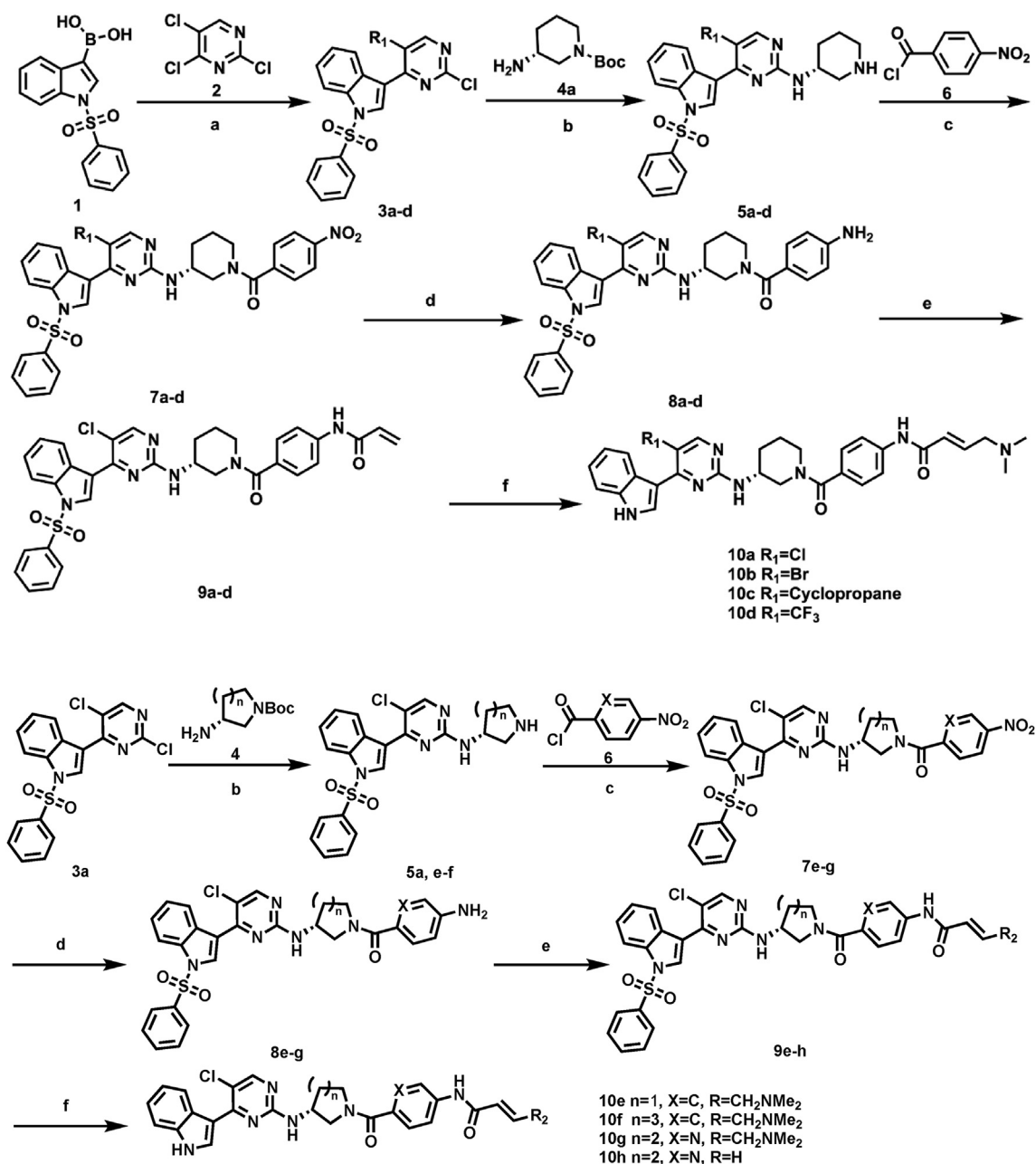


Fig. 1. Structures of THZ1 and THZ531.



Scheme 1. Synthesis of 10a-10h.^a Reagents and conditions: (a) Pd(PPh₃)₄, Na₂CO₃, CH₃CN, 80 °C; (b) DIPEA, NMP, 140 °C; (c) HATU, DIPEA, DMF; (d) SnCl₂, MeOH, Ethyl Acetate, 80 °C; (e) Acryloyl chloride, DIPEA, CH₃CN, 0 °C. Or (*E*)-4-bromobut-2-enoyl chloride, DIPEA, CH₃CN, 0 °C; Dimethylamine, CH₃CN; (f) NaOH, dioxane.

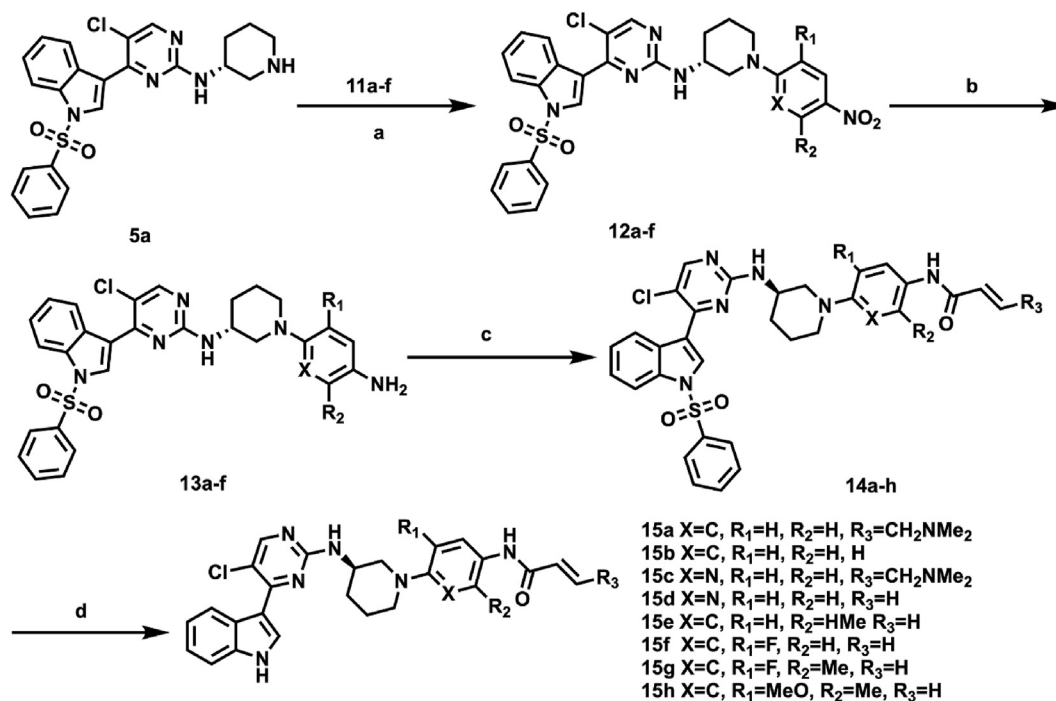
compared to THZ531 (Table 3). In addition, we observed improved selectivity against CDK9 and CDK2. Next, we explored whether the stereochemistry of the ether connection impacts the activity and we therefore synthesized compound **22c** with an *S* configuration. Although compound **22c** retained the potency of BSJ-01-175 on CDK12/13, it also exhibited increased activity on both CDK2 and CDK9. Finally, the exploration of substitution on the phenyl ring turned out to be much less tolerated compared to the **15** series as exemplified by a loss of potency with compound **22d**, in which a F group was installed at 2-position. Collectively, our medicinal chemistry efforts have resulted in a group of compounds with improved potency and selectivity over our starting point (THZ531). These compounds include **10h**, **15b**, **15f**, **15g**, **15h**, **20b** and BSJ-01-175, which were then further evaluated in mouse liver microsomal stability (MLM) assay (Table 4). Out of this collection, BSJ-01-

175 showed the best microsomal stability. Therefore BSJ-01-175 was chosen for further biochemical and structural characterization as well as cell-based assays and animal studies.

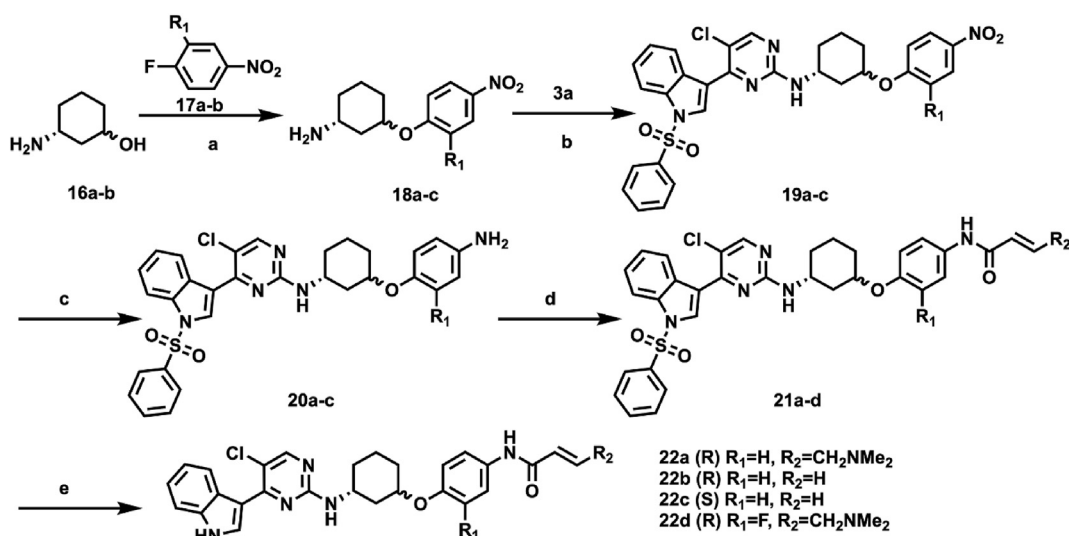
2.3. Characterization of BSJ-01-175

2.3.1. BSJ-01-175 covalently binds to CDK12 at cysteine 1039

To assess whether BSJ-01-175 reacts covalently with CDK12, we incubated CDK12/Cyclin K complex with a 10-fold molar excess of compound BSJ-01-175 and analyzed reaction products by LC-MS. After the reaction, CDK12, but not Cyclin K, showed an increase in mass consistent with covalent addition of a single molecule of BSJ-01-175 (Fig. 2A). To identify the site of modification, the labeled protein complex was digested with gluc protease, and proteolytic fragments were analyzed by CE-MS, revealing exclusive



Scheme 2. Synthesis of 15a-15h^a. ^aReagents and conditions: (a) DIPEA, DMF, 80 °C; (b) SnCl₂, MeOH, Ethyl Acetate, 80 °C; (c) Acryloyl chloride, DIPEA, CH₃CN, 0 °C. Or (*E*)-4-bromobut-2-enoyl chloride, DIPEA, CH₃CN, 0 °C; Dimethylamine, CH₃CN; (d) NaOH, dioxane.



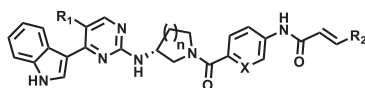
Scheme 3. Synthesis of 22a-22e^a. ^aReagents and conditions: (a) NaH, DMF, 0 °C–25 °C; (b) DIPEA, NMP, 140 °C; (c) SnCl₂, MeOH, Ethyl Acetate, 80 °C; (d) Acryloyl chloride, DIPEA, CH₃CN, 0 °C. Or (*E*)-4-bromobut-2-enoyl chloride, DIPEA, CH₃CN, 0 °C; Dimethylamine, CH₃CN; (e) NaOH, dioxane.

modification of Cys1039 (Fig. 2B).

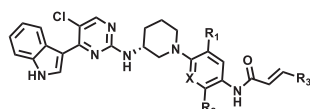
2.3.2. Structure determination of CDK12/CycK with BSJ-01-175

The specific interaction of compound BSJ-01-175 with CDK12 and the formation of a covalent bond to Cys1039 was analyzed structurally. We determined the crystal structure of CDK12–Cyclin K in complex with BSJ-01-175 to 3.0 Å resolution with excellent stereochemistry (see Supplementary Table S2 for diffraction data collection and refinement statistics). As observed before [18,20], we found two CDK-cyclin complexes per asymmetric unit, with the CDK12 molecule forming a covalent bond between Cys1039 and BSJ-01-175 (Fig. 3A and Supplementary Fig. S1). Within a shell of

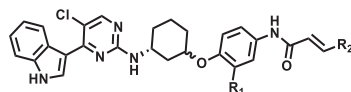
3.8 Å, twelve CDK12 residues were found to make direct contacts with BSJ-01-175, with one additional water mediated contact between the amino group of Lys756, the backbone amide of Asp877, and the indole ring amine of the compound (Fig. 3B). A small twist of the cyclohexane group of BSJ-01-175 induces a rotamer shift in the phenyl ring in the linker region of the compound, leading to a different orientation of the acrylamide moiety in the two CDK-cyclin complexes of the asymmetric unit compared to THZ531 (see below). In both complexes, the C-terminal extension helix α K of CDK12 is displaced from the kinase lobe structure allowing Cys1039 to reorient toward the ATP-binding site for reacting with BSJ-01-175 (Supplementary Fig. S2). The aminopyrimidine of BSJ-

Table 1
IC50 values for compounds 10a-10 g against CDK2,7,9,12 and 13.

Compound	n	X	R ₁	R ₂	IC ₅₀ (nM)				
					CDK2	CDK7	CDK9	CDK12	CDK13
10a (THZ531)	2	C	Cl	CH ₂ NMe ₂	1300	452	193	482.6	657.1
10b	2	C	Br	CH ₂ NMe ₂	1000	115	184	225.6	572.6
10c	2	C		CH ₂ NMe ₂	>10,000	625	>10,000	9979	>10,000
10d	2	C	CF ₃	CH ₂ NMe ₂	10,000	>10,000	>10,000	>10,000	10,000
10e	1	C	Cl	CH ₂ NMe ₂	49.3	6.33	14.2	68.7	50.2
10f	3	C	Cl	CH ₂ NMe ₂	339	388	1220	1450	1831
10 g	2	N	Cl	CH ₂ NMe ₂	3870	402	658	764.9	1636
10h	2	N	Cl	H	3390	919	530	231.7	798.9

Table 2
IC50 values for compounds 15a-15h against CDK2,7,9,12 and 13.

Compound	X	R ₁	R ₂	R ₃	IC ₅₀ (nM)				
					CDK2	CDK7	CDK9	CDK12	CDK13
15a	C	H	H	CH ₂ NMe ₂	623	69.5	155	166.7	177.6
15b	C	H	H	H	3550	162	171	93.6	123
15c	N	H	H	CH ₂ NMe ₂	492	74	87.7	35.4	186.1
15d	N	H	H	H	1940	433	121	67.6	120
15e	C	H	Me	H	1100	197	165	142.3	238.8
15f	C	F	H	H	4020	318	436	87.6	126.6
15g	C	F	Me	H	266	118	230	130.5	203.8
15h	C	MeO	Me	H	3360	403	522	293.2	4385

Table 3
IC₅₀ values for compounds 22a-22e against CDK2,7,9,12 and 13.

Compound	Chirality	R ₁	R ₂	IC ₅₀ (nM)				
				CDK2	CDK7	CDK9	CDK12	CDK13
22a (BSJ-01-175)	R	H	CH ₂ NMe ₂	4510	187	367	156	282.6
22b	R	H	H	>10,000	587	585	155.1	328.1
22c	S	H	CH ₂ NMe ₂	650	112	132	181	182
22d	R	F	CH ₂ NMe ₂	3570	269	286	857.2	484.2

Table 4
Mouse liver microsomal half-life.

Compound	MLM T _{1/2} (min)	Compound	MLM T _{1/2} (min)
10h	3.5	15h	4.3
15b	7.2	BSJ-01-175	8
15f	7.6	20b	5.4
15g	3.9		

01-175 forms two hydrogen bonds to the backbone of Met816 of the kinase hinge region, while the cyclohexane and phenyl rings

mediate further hydrophobic interactions, stacked between Leu866 of the antiparallel β -strand preceding the kinase T-loop, and Ile733 of the N-lobe β 1 strand, respectively (Fig. 3B). The electron density map of the following exposed linker sites is poorly defined, except for the side chain of Cys1039, which is again clearly visible with its covalent bond to the acrylamide moiety of BSJ-01-175 (Supplementary Fig. S1A).

To compare BSJ-01-175 and THZ531 binding modes, we determined the crystal structure of the latter bound to CDK13/Cyclin K at 2.36 Å resolution (Fig. 3C, see Table S2 for refinement statistics). As seen before and described above, two cyclin-kinase complexes

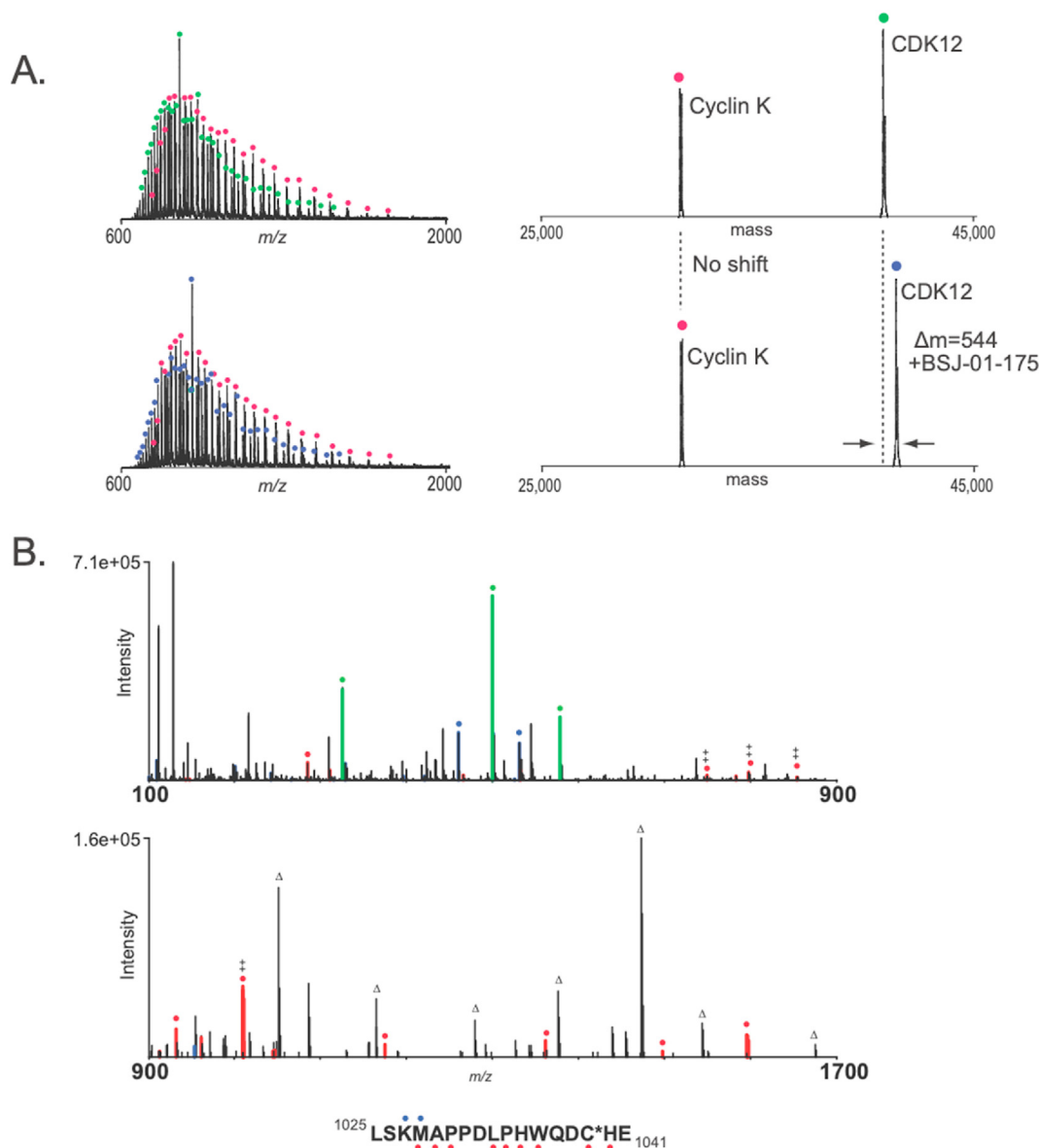


Fig. 2. CDK12 is labeled by BSJ-01-175 at Cys1039. (A) Mass spectra (left) and zero-charge mass spectra (right) of CDK12/cyclin K complex treated with (top) DMSO or (bottom) a 10-fold excess of BSJ-01-175 for 1 h at room temperature. Mass spectral peaks are labeled with glyphs and correspond to cyclin K (red), unmodified CDK12 (green), and CDK12 covalently labeled with BSJ-01-175 (blue). Cyclin K is unaffected by compound treatment, while CDK12 protein exhibits an increase in mass consistent with modification by a single molecule of BSJ-01-175. (B) MS/MS spectrum of CDK12 peptide¹⁰²⁵LSKMAPPDLPHWQDC¹⁰⁴¹ modified with BSJ-01-175 indicates covalent labeling of Cys1039. Ions of types b and y are indicated with blue and red glyphs, respectively. Inhibitor related ions [26] are marked with green glyphs. Δ peak corresponding to neutral loss of BSJ-01-175.

were found in the asymmetric unit [21]. The twist of the THZ531 piperidine ring in these two forms is more pronounced than what we observed for the cyclohexane ring in BSJ-01-175 (Fig. 3D). This results in a significantly different orientation of the acrylamide linker region (Supplementary Fig. S3). These conformational differences are possible due to the high flexibility in the kinase extension helix α K harboring the cysteine site that is targeted by the covalent linkage (Supplementary Fig. S4). We observed that while in one of the forms the side chain of Gln1015 participates in a hydrogen-bond network between the amine backbone of Asp797 and the carbonyl group of the THZ531 acrylamide moiety, the other form features THZ531 that uses its linker region to form hydrophobic contacts to the N-lobe β 1 strand (Supplementary Fig. S3B).

The variable linker region to the cysteine becomes also apparent from an overlay of the two CDK12 crystal structures bound to THZ531 (PDB accession code 5ACB) [18] or bound to BSJ-01-175

(Fig. 4A). A superimposition with the crystal structure of CDK12 bound to ADP (4NST) [20] instead reveals that the cyclohexane moiety of BSJ-01-175 adopts a similar position as the imidazole ring of His1040 directly preceding the C-terminal extension helix (Fig. 4B). The conformational differences of the linker regions to the bound cysteines may thus give rise to the improved stability of BSJ-01-175 compared to THZ531.

2.3.3. BSJ-01-175 is a selective CDK12/13 inhibitor

To assess the selectivity of BSJ-01-175, we used the KiNativ approach [22] that reports on how well a compound blocks irreversible binding of a non-specific ADP(ATP)-biotin probe to cellular kinases. In these experiments, Kelly cells were pre-exposed to 1 μ M of BSJ-01-175, then lysed, treated with the irreversible ADP(ATP)-biotin probe and pulled down via an affinity column. These results were compared to the DMSO treated negative control as a

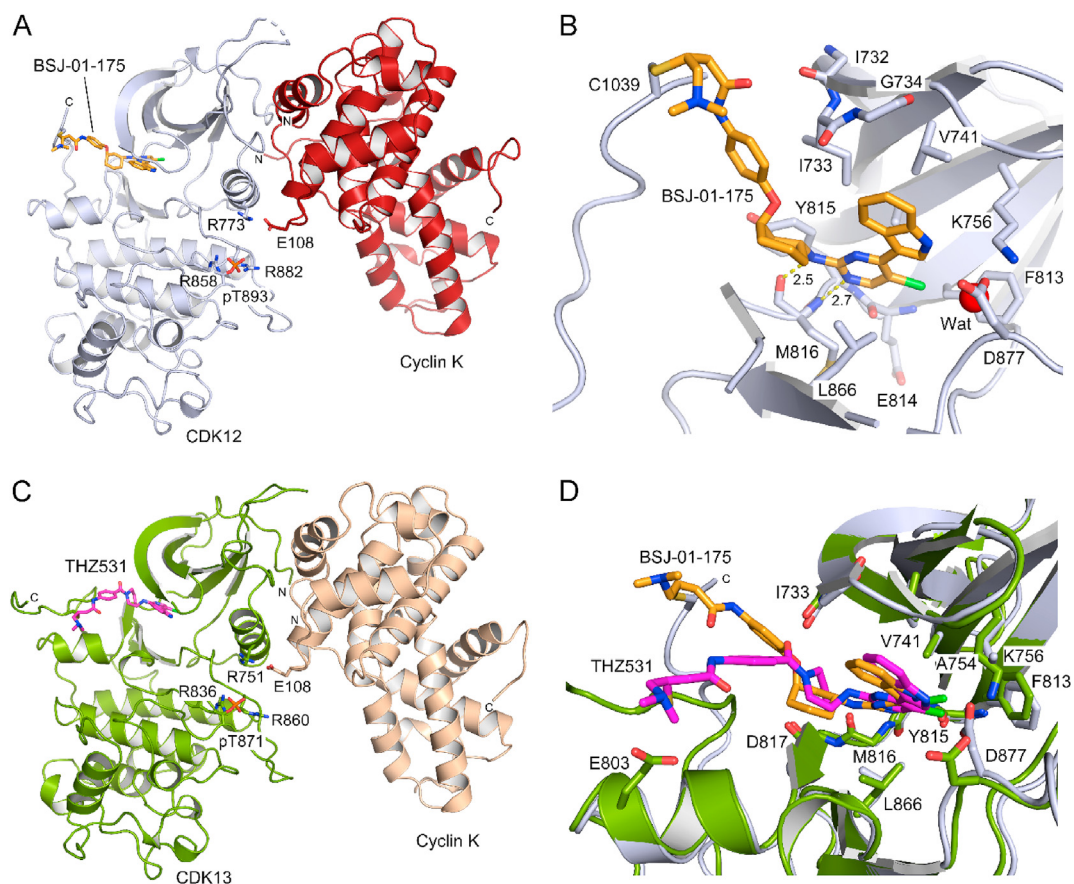


Fig. 3. Crystal structures of CDK12/Cyclin K bound to BSJ-01-175 and CDK13/Cyclin K bound to THZ531. (A) Complex structure of CDK12/Cyclin K bound to BSJ-01-175 (PDB accession code 7NXK). The phosphorylated threonine in the T-loop of the kinase and its coordinating arginine residues are indicated. (B) Close up of the interactions of BSJ-01-175 with the kinase N-lobe of CDK12. Hydrogen bonds of the aminopyrimidine are highlighted. (C) Structure of CDK13/Cyclin K bound to THZ531 (PDB accession code 7NXJ). (D) Overlay of the CDK12/Cyclin K structure with CDK13/Cyclin K bound to BSJ-01-175 and THZ531, respectively. The variable conformations of the acrylamide moiety binding covalently to the conserved cysteine residues are shown.

benchmark. As shown in Table 5, most of the protein kinases (total 270 proteins, Supplementary Dataset 1) were not affected (BSJ-01-175 blocked less than 50% of ADP(ATP)-biotin probe binding), whereas BSJ-01-175 was able to protect 75% of CDK12 from probe binding. Although DNAPK, RSK2 and CDK7 displayed a degree of protection higher than 50%, only CDK7 has a targetable cysteine and biochemically, weak inhibitory IC_{50} values against both DNPAK ($>10,000$ nM) and RSK2 (4500 nM) were detected, suggesting BSJ-01-175 is a weak inhibitor for both proteins. Therefore, we carefully examined the selectivity for CDK12/13 over CDK7, as discussed in the next section.

2.3.4. BSJ-01-175 inhibited CDK12/13 activity and the downstream signaling

We employed BSJ-01-175 in a series of cell-based assays to examine its cellular activity, and establish whether the phenotype is CDK12/13-inhibition dependent. First, we carried out a rescue experiment using THZ1-biotin, a probe that binds CDK7/12/13 covalently, allowing their pulldown via streptavidin beads. Here, Jurkat cells treated with increasing amounts of BSJ-01-175 for 6 h were lysed and then exposed to 1 μ M of THZ1-biotin. The pulldown samples from streptavidin beads were immuno-blotted with the antibodies for cyclin K and cyclin H (a CDK7 binding partner), as surrogate readouts for CDK12/13 and CDK7, respectively. As shown in Fig. 5A, BSJ-01-175 competed off THZ1-biotin binding with CDK12/13, while leaving CDK7 untouched at concentration of

500 nM. Compared to THZ531, which engages CDK7 at 1 μ M, BSJ-01-175 exhibited mild engagement even at higher concentrations (5 μ M). The irreversibility on CDK12/13's binding by BSJ-01-175 in cellular context was well-demonstrated by sustained engagement even at 24 h after a washout experiment (Fig. 5B). Next, to understand how the target engagement affects CDK12/13 downstream signaling, we examined phosphorylation levels on Ser2 of RNA pol II. With 500 nM of BSJ-01-175, p-Ser2 was significantly reduced, whereas Ser5 and Ser7, two non-CDK12/13 phosphorylation sites remained unchanged. At higher concentrations, BSJ-01-175 reduced the protein levels of p-Ser2/5/7, as well as total RNA pol II (Fig. 5C). As a transcriptional regulator, loss of CDK12 function by BSJ-01-175 was expected to cause transcriptional defects on specific DDR genes regulated by this kinase. We therefore measured BRCA1 and BRCA2 expression in Jurkat cells pretreated with BSJ-01-175 for 4 h. As shown in Fig. 5D, both BRCA 1 and 2 genes were downregulated to below 30% of DMSO control. Lastly, we exposed previously generated Cys1039Phe mutant Kelly cells, resistant to covalent CDK12/13 inhibitors that target Cys1039 [23], to BSJ-01-175 and observed a 5-fold increase in cell viability compared to the wild type (WT) (Fig. 6) indicating strong dependence on covalent bond formation with Cys1039.

2.3.5. BSJ-01-175 suppresses tumor growth of Ewing sarcoma

Our previous study has shown that a pan CDK7/12/13 covalent inhibitor THZ1 alone or combination with PARP inhibitor Olaparib

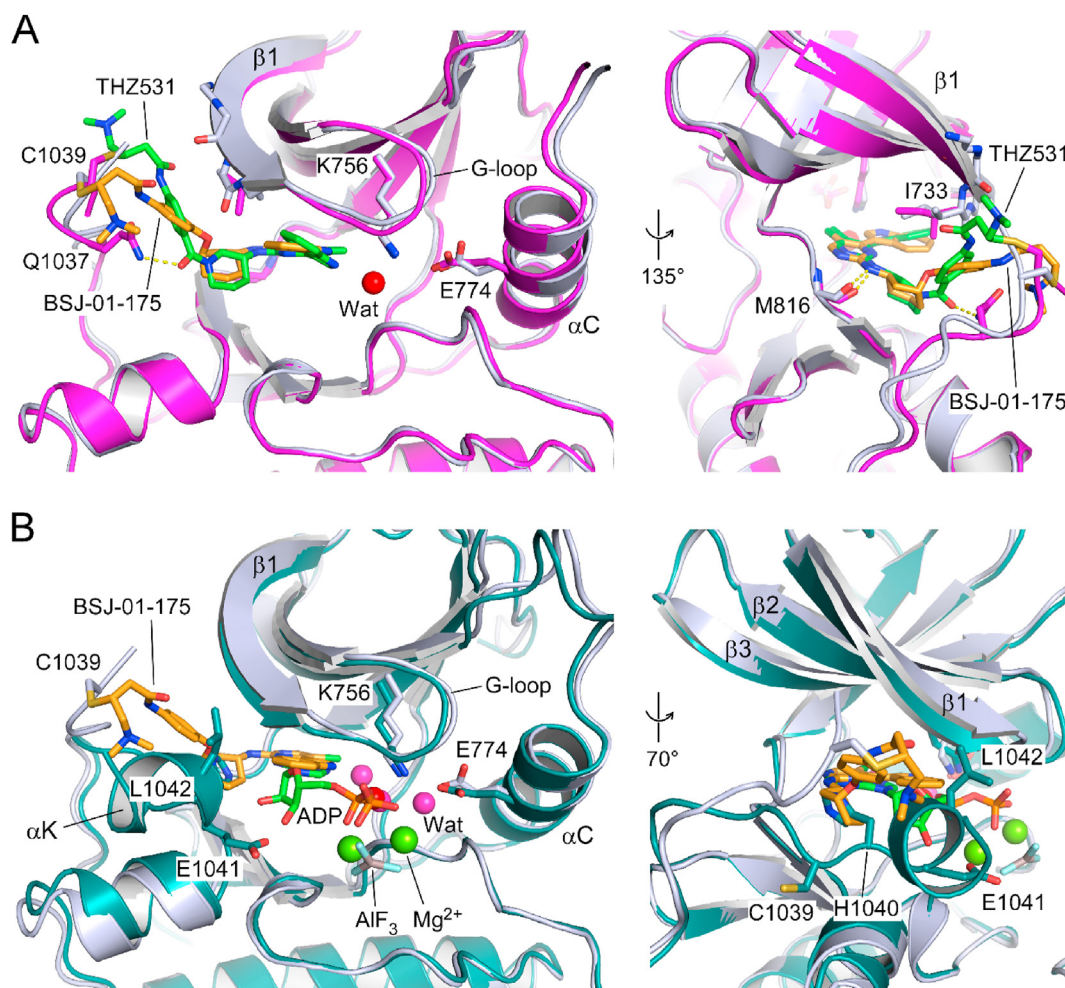


Fig. 4. Overlay of CDK12 crystal structures in complex with BSJ-01-175, THZ531 or ADP•AlF₃•2Mg²⁺. (A) Superimposition of the two CDK12 structures complexed with BSJ-01-175 (7NXX; chain A, light blue/orange) or THZ531 (5ACB; chain C, magenta/green). Key residues and important secondary structure elements are indicated. (B) Superimposition of the CDK12–BSJ-01-175 structure (7NXX; chain A, light blue/orange) and the CDK12–ADP•AlF₃•2Mg²⁺ nucleotide bound complex (4NST; chain A, teal/green). The imidazole ring of H1040 from the DCHL motif at the beginning of the C-terminal extension helix α K adopts a similar position as the cyclohexane ring in BSJ-01-175 (right picture).

can suppress the growth of Ewing Sarcoma *in vivo* [17]. To understand whether this efficacy can be recapitulated with a selective CDK12/13 inhibitor, we first measured the antiproliferative activity of BSJ-01-175 in TC71 Ewing sarcoma cells, and observed a slight decrease of activity compared to THZ531 (Fig. 7A).

Next, the pharmacokinetic (PK) properties of BSJ-01-175 was examined following two routes of administration (IV and PO), and displayed a moderate stability with $T_{1/2}$ of 2.25 h, a low clearance (24.9 mL/min/kg), and 17% oral bioavailability (Table 6). Given these promising results, we administrated BSJ-01-175 with IP dosing of 10 mg/kg three doses weekly to Ewing sarcoma PDX model derived from TC71 cells. Compared to the vehicle control, BSJ-01-175 led to a significant suppression of tumor growth throughout 3 weeks of drug treatment period (Fig. 7B). However, we did observe weight loss toxicity (Fig. 7C), requiring dosing protocol to be adjusted to two three-day treatment holidays at Day 10 and Day 16. Whether body weight loss is caused by CDK12/13 inhibition or a metabolic liability of BSJ-01-175 remains to be addressed.

3. Conclusion

Targeting a unique cysteine with a well-designed covalent inhibitor represents a powerful avenue to achieve highly selective

kinase inhibitors. For example, THZ1, the first covalent inhibitor of the CDK family, inhibits three CDKs, CDK7, CDK12 and CDK13, by reacting with cysteines that are located at similar positions by sequence alignment but arranged differently in 3-dimensional space. Our subsequent work produced THZ531, a selective CDK12/13 inhibitor that features 3-amino-piperidine moiety that is responsible for imparting selectivity for CDK12/13 relative to CDK7 [18]. Here, we describe results of our med-chem efforts and identify several compounds of interest. Most significantly, we report and characterize BSJ-01-175 that exhibited an exquisite selectivity profile at a concentration that completely inhibited CDK12-regulated signaling. Compared to THZ531, BSJ-01-175 was developed to include DMA, a group known to improve solubility and metabolic stability, resulting in a 3-fold activity improvement and suitable stability for animal studies. Importantly, we show that BSJ-01-175 demonstrates efficacy in Ewing sarcoma PDX model. This study also led to compound **15h**, a potential lead for development of CDK12 specific inhibitor. Further modifications of BSJ-01-175 or its analog **15h** are needed to develop specific covalent CDK12 or 13 inhibitors, and/or optimize the current series into less toxic compounds not resulting in the body weight loss induced by BSJ-01-175. Taken together, our study confirms that the THZ1 scaffold can be optimized both in terms of selectivity and pharmacological

Table 5
Intracellular KiNativ™ profiling assay identifies CDK12 as major target of BSJ-01-175.

Kinase	Compound BSJ-01-175 (1 μM)
CRK7/CDK12	76.8
DNAPK	60.9
RSK2 domain1	58.6
CDK7	57.5
RSK1 domain1, RSK2 domain1, RSK3 domain1	46.0
JNK1, JNK2, JNK3	45.9
STLK6	44.5
MPSK1	42.4
RSK3 domain1	41.6
MSK2 domain1	40.3
CDK7	39.2
DNAPK	38.3
CaMK4	38.2
MSK2 domain1	37.8
RAF1	37.8
RSK1 domain1	35.4
LOK	33.9

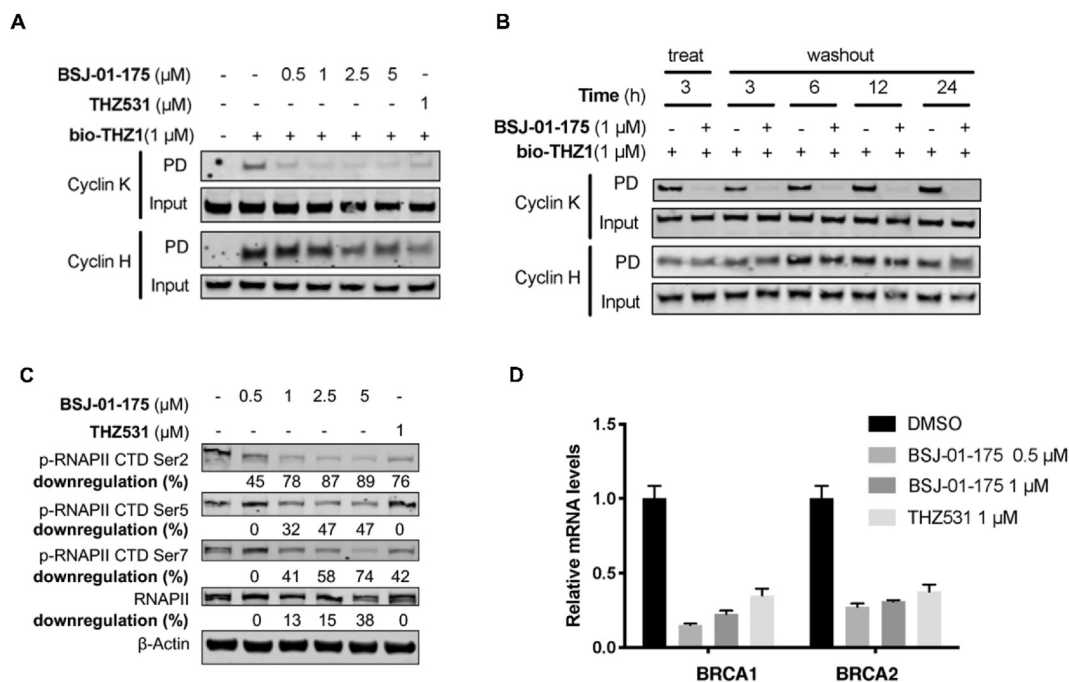


Fig. 5. BSJ-01-175 specifically targets CDK12/13 and suppresses the transcription of BRCA1 and BRCA2. (A) Competitive pulldown assay in Jurkat cells treated with BSJ-01-175 at indicated concentrations for 6 h. Cell lysates were incubated with bio-THZ1 that competes for the binding pocket of the target kinase. Western blotting showing the pulldown (PD) or input (total lysate) of Cyclin H and Cyclin K. (B) BSJ-01-175 binds intracellular CDK12-cyclin K complexes 24 h after washout in competitive pulldown assay. Jurkat cells were treated with BSJ-01-175 for 3 h, followed by washout for indicated times. Cell lysates were incubated with bio-THZ1 that competes for the binding pocket of the target kinase. Western blotting showing the pulldown (PD) or input (total lysate) of Cyclin H and Cyclin K. (C) BSJ-01-175 inhibits phosphorylation of RNA pol II CTD and downregulates total RNA pol II CTD in Jurkat cells. Cells were treated with BSJ-01-175 or THZ531 for 6 h and cell lysates were subjected to immunoblotting analysis. THZ531 was used as a positive control. (D) RT-qPCR of BRCA1/2 gene expression following BSJ-01-175 or THZ531 treatment (4 h) in Jurkat cells. Data are presented as the mean ± SEM (n = 3). The figure is one representation from three independent experiments.

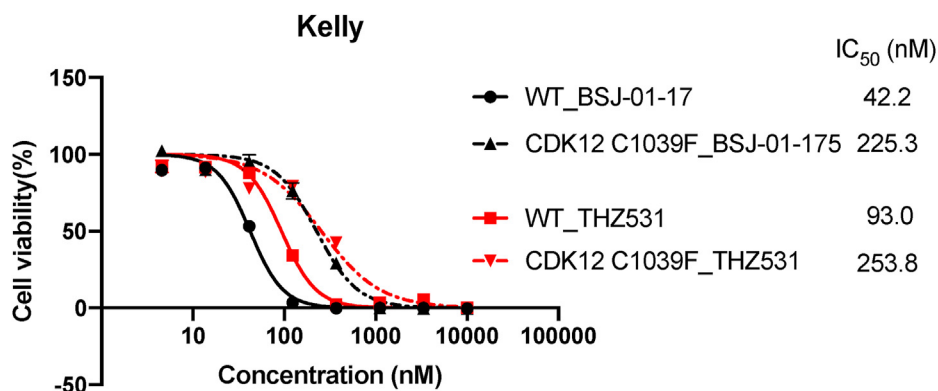


Fig. 6. Anti-proliferation activity of BSJ-01-175 on Kelly cells with WT CDK12 or C1039F mutant. Cell proliferation assay in WT and CDK12C1039F Kelly cells. Cells were treated with the indicated compounds for 72 h and subjected to CellTiter-Glo assay. Data are presented as mean \pm SEM (n = 3). The figure is one representation from three independent experiments.

properties, and suggest that further work in this area will likely lead to clinically relevant chemical matter.

4. Experimental section

4.1. Chemistry

Unless otherwise noted, reagents and solvents were obtained from commercial suppliers and were used without further purification. ¹H NMR spectra were recorded on 500 MHz (Bruker A500), and chemical shifts are reported in parts per million (ppm, δ) downfield from tetramethylsilane (TMS). Coupling constants (J) are reported in Hz. Spin multiplicities are described as s (singlet), br (broad singlet), d (doublet), t (triplet), q (quartet), and m (multiplet). Mass spectra were obtained on a Waters Micromass ZQ instrument. Preparative HPLC was performed on a Waters Sunfire C18 column (19 \times 50 mm, 5 μ M) using a gradient of 5–95% methanol in water or acetonitrile in water containing 0.05% trifluoroacetic acid (TFA) over 22 min (28 min run time) or 35 min (45 min run time) at a flow rate of 20 mL/min. All of the final compounds reported had purities greater than 95% based on ¹H nuclear magnetic resonance (NMR) and liquid chromatography–mass spectrometry (LC–MS).

4.1.1. General procedures for synthesis of compound 10a-10h

To a solution of 2,4,5-trichloropyrimidine **2a** (378 mg, 2 mmol) in 5 mL of CH₃CN under N₂ was added 1-(phenylsulfonyl)-1H-indol-3-ylboronic acid **1** (602 mg, 2 mmol) and 2 mL of saturated aqueous Na₂CO₃. The mixture was degassed 3 times before the addition of Pd(PPh₃)₄ (115 mg, 0.1 mmol). After degassing a further 3 times, the mixture was heated to 80 °C for 2 h. The resulting precipitate was filtered and washed with water and ether to afford the desired compound 3-(2,5-dichloropyrimidin-4-yl)-1-(phenylsulfonyl)-1H-indole **3a** as a light grey solid (687 mg, 85%). LC-MS: *m/z* 404 (M+H).

To a solution of **3a** (403 mg, 1 mmol) in 5 mL of NMP was added *tert*-butyl (R)-3-aminopiperidine-1-carboxylate **4a** (200 mg, 1 mmol) and DIPEA (0.52 μ L, 3 mmol). The solution was heated for 2 h at 130 °C. The cooled solution was diluted with 100 mL of CHCl₃ and 2-PrOH (4:1) and then washed with water. The organic phase was then evaporated to give a brown crude which was dissolved in 3 mL of DCM, followed by a slow addition of 3 mL of TFA at 80 °C. After 30 min stirring at room temperature, the solvent was then removed. The residue was purified by silica gel chromatography column with DCM/methanol (10/1) to give the product (R)-5-chloro-4-(1-(phenylsulfonyl)-1H-indol-3-yl)-N-(piperidin-3-yl)pyrimidin-2-amine **5a** (350 mg, 76% in two steps). LC-MS: *m/z* 468

(M+H).

To a stirred solution of **5a** (327 mg, 0.7 mmol) in 5 mL of pyridine was added 4-nitrobenzoyl chloride **6a** (126 mg, 0.7 mmol) and then was heated to 80 °C. The reaction mixture was stirred for 2 h and then was cooled to room temperature and concentrated under reduced pressure. The resulting crude was purified by silica gel column with DCM/methanol (10/1) to give the desired compound (R)-3-((5-chloro-4-(1-(phenylsulfonyl)-1H-indol-3-yl)pyrimidin-2-yl)amino)piperidin-1-yl)(4-nitrophenyl)methanone **7a** (315 mg, 73%). LC-MS: *m/z* 617 (M+H).

The nitro compound **7a** (308 mg, 0.5 mmol) was suspended in 15 mL of ethyl acetate/methanol (5:1), followed by addition of SnCl₂ (948 mg, 5 mmol). After stirring for 2 h at 80 °C, the reaction mixture was cooled down to room temperature and poured onto saturated aqueous NaHCO₃. The mixture was stirred for 10 min followed by extraction with 100 mL of CHCl₃ and 2-propanol (4:1). The organic layer was washed with water and brine, dried over sodium sulfate, filtered through a pad of Celite and concentrated under reduced pressure. The resulting crude was purified by silica gel column with DCM/methanol (10/1) to provide the desired compound (R)-4-(aminophenyl)-3-((5-chloro-4-(1-(phenylsulfonyl)-1H-indol-3-yl)pyrimidin-2-yl)amino)piperidin-1-yl)methanone **8a** (161.4 mg, 55%). LC-MS: *m/z* 587 (M+H).

To the solution of the compound **8a** (117.4 mg, 0.2 mmol) in 5 mL of CH₃CN was added DIPEA (70 μ L, 0.4 mmol). The reaction mixture was cooled down to 0 °C and then treated with 4-bromobut-2-enoyl chloride (36.4 mg, 0.2 mmol) or acryloyl chloride (18 mg, 0.2 mmol) in DCM. The reaction mixture was stirred for 10 min at 0 °C to give the acrylamide **9h** (LC-MS: *m/z* 641 (M+H)), and bromide intermediate. Dimethylamine in THF (1 M, 2.0 mL) was then added to the bromide intermediate solution. The resulting mixture was warmed up to room temperature, stirred for 30 min and then concentrated under reduced pressure. The resulting crude was purified by reverse phase HPLC (5–95% MeOH in H₂O) to give the desired compound **9a** (91 mg, 65%). LC-MS: *m/z* 698 (M+H).

The compound **9a** (70 mg, 0.1 mmol) was dissolved in 2 mL of 1,4-dioxane and 2 mL of 1 M aqueous NaOH. The solution was allowed to stir at room temperature for 2 h followed by neutralization with 2 mL of 4 M HCl in Dioxane. The solution was then extracted with 30 mL of CHCl₃ and 2-propanol (4:1) and was washed with water. The removal of solvent provided the crude which was purified by reverse phase HPLC (5–95% MeOH in H₂O) to give (R,E)-N-(4-(3-((5-chloro-4-(1H-indol-3-yl)pyrimidin-2-yl)amino)piperidine-1-carbonyl)phenyl)-4-(dimethylamino)but-2-enamide **10a** (25 mg, 43%). LC-MS: *m/z* 558 (M+1), ¹H NMR (500 MHz, DMSO-*d*₆) 11.83 (s, 1H), 10.94 (s, 1H), 10.41 (s, 1H), 8.53 (s,

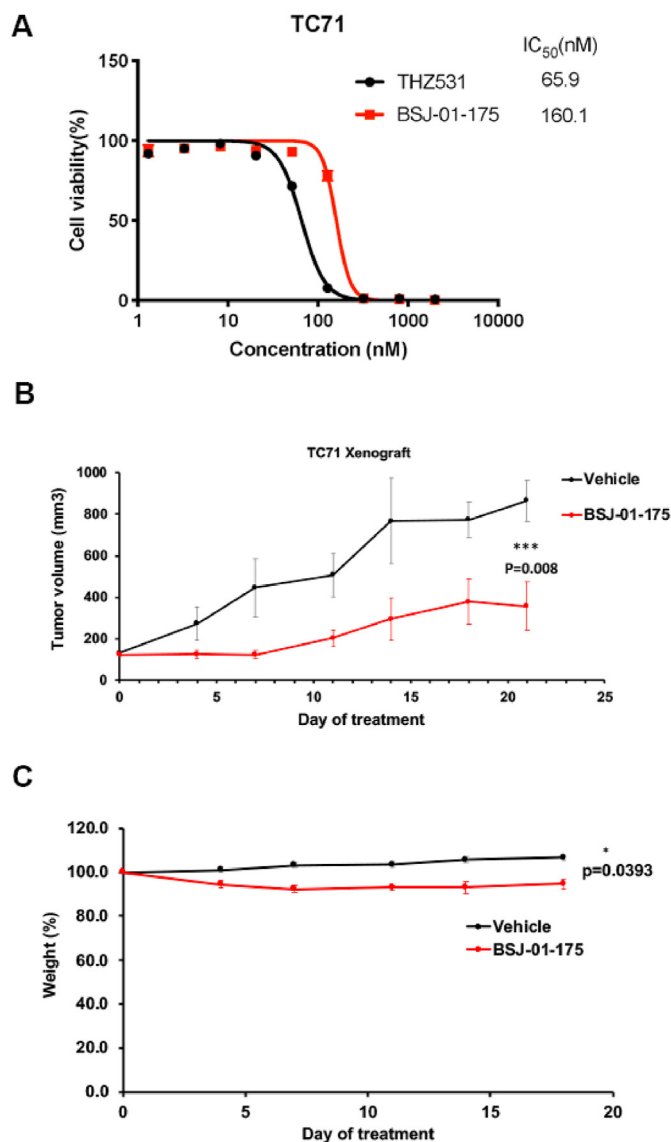


Fig. 7. BSJ-01-175 suppresses tumor growth of Ewing sarcoma. (A) Antiproliferation of BSJ-01-175 on TC71 cells, data are presented as the mean \pm SEM (n = 3). The figure is one representation from two independent experiments. (B) Tumor volume measurements of a subcutaneous TC71 xenograft mouse model of Ewing sarcoma treated with vehicle or 10 mg/kg BSJ-01-175 IP qd. Treatment was stopped on day 21. Data are plotted as mean values \pm SD. *p value < 0.05, 2-way ANOVA with Tukey post hoc test. (C) Relative weight measurements of mice in B. Data are plotted as mean values \pm SD. ***p value < 0.001. 2-way ANOVA with Tukey post hoc test. Mice used in (B) and (C) are 5 in vehicle group and 5 in BSJ-01-175 group.

1H), 8.44 (s, 1H), 8.25 (s, 1H), 7.67 (d, J = 7.0 Hz, 1H), 7.52 (d, J = 8.0 Hz, 1H), 7.36 (d, J = 8.5 Hz, 2H), 7.22 (t, J = 8.0 Hz, 1H), 7.16 (d, J = 8.0 Hz, 1H), 6.83 (m, 1H), 6.52 (d, J = 15.0 Hz, 1H), 4.02 (br, 2H), 3.93–3.80 (m, 3H), 3.20 (br, 2H), 2.80 (s, 6H), 2.10 (m, 1H), 1.86 (m, 1H), 1.71 (m, 1H), 1.61 (m, 1H).

(R,E)-N-(4-(3-((5-bromo-4-(1H-indol-3-yl)pyrimidin-2-yl)

amino)piperidine-1-carbonyl)phenyl)-4-(dimethylamino)but-2-enamide (10b) LC-MS: *m/z* 602 (M+H). ¹H NMR (500 MHz, DMSO-*d*₆) δ 11.82 (s, 1H), 10.50 (s, 1H), 10.09 (s, 1H), 8.66–8.25 (m, 2H), 7.69 (br, 2H), 7.48 (d, J = 8.1 Hz, 1H), 7.38 (br, 2H), 7.25–7.06 (m, 2H), 6.83–6.72 (m, 1H), 6.54–6.41 (m, 1H), 4.44 (br, 1H), 3.95 (br, 4H), 3.13 (br, 2H), 2.80 (s, 6H), 2.06 (br, 1H), 1.95–1.78 (m, 1H), 1.66 (s, 1H), 1.54 (s, 1H).

(R,E)-N-(4-(3-((5-cyclopropyl-4-(1H-indol-3-yl)pyrimidin-2-yl)amino)piperidine-1-carbonyl)phenyl)-4-(dimethylamino)but-2-enamide (10c) LC-MS: *m/z* 564 (M+H). ¹H NMR (500 MHz, DMSO-*d*₆) δ 11.89 (s, 1H), 10.52 (s, 1H), 10.07 (s, 1H), 8.68 (br, 2H), 8.08 (s, 1H), 7.68 (br, 1H), 7.55 (d, J = 8.0 Hz, 1H), 7.41 (s, 1H), 7.30–7.11 (m, 2H), 6.87–6.67 (m, 1H), 6.56–6.40 (m, 1H), 3.96 (br, 4H), 3.54 (br, 3H), 2.82 (s, 6H), 2.18–2.08 (m, 1H), 2.03 (br, 1H), 1.87 (br, 1H), 1.75 (br, 1H), 1.60 (br, 1H), 1.13–0.93 (m, 2H), 0.74–0.52 (br, 2H).

(R,E)-N-(4-(3-((4-(1H-indol-3-yl)-5-(trifluoromethyl)pyrimidin-2-yl)amino)piperidine-1-carbonyl)phenyl)-4-(dimethylamino)but-2-enamide (10d) LC-MS: *m/z* 592 (M+H). ¹H NMR (500 MHz, DMSO-*d*₆) δ 11.88 (s, 1H), 10.50 (br, 1H), 9.83 (s, 1H), 8.50 (s, 1H), 8.45–8.22 (m, 2H), 7.74 (br, 2H), 7.53–7.34 (m, 2H), 7.23–7.08 (m, 2H), 6.95 (br, 1H), 6.83–6.63 (m, 1H), 6.44 (br, 1H), 4.53 (br, 2H), 3.96 (br, 4H), 3.57 (br, 1H), 2.80 (s, 6H), 1.99–1.88 (m, 1H), 1.82–1.70 (m, 1H), 1.69–1.56 (br, 1H).

(R,E)-N-(4-(3-((5-chloro-4-(1H-indol-3-yl)pyrimidin-2-yl)amino)pyrrolidine-1-carbonyl)phenyl)-4-(dimethylamino)but-2-enamide (10e) LC-MS: *m/z* 544 (M+H). ¹H NMR (500 MHz, DMSO-*d*₆) δ 11.87 (s, 1H), 10.49 (s, 1H), 9.88 (s, 1H), 8.47 (s, 1H), 8.63 (br, 1H), 8.29 (s, 1H), 7.80–7.42 (m, 3H), 7.29–7.15 (s, 2H), 7.07 (s, 1H), 6.82–6.69 (m, 1H), 6.63–6.30 (m, 1H), 4.65–4.30 (br, 2H), 3.94 (br, 2H), 3.47 (br, 2H), 2.80 (s, 6H), 2.23 (s, 1H), 2.15–1.93 (m, 1H), 1.31–1.04 (m, 1H).

(R,E)-N-(4-(3-((5-chloro-4-(1H-indol-3-yl)pyrimidin-2-yl)amino)azepane-1-carbonyl)phenyl)-4-(dimethylamino)but-2-enamide (10f) LC-MS: *m/z* 572 (M+H). ¹H NMR (500 MHz, DMSO-*d*₆) δ 11.86 (s, 1H), 10.44 (s, 1H), 9.82 (s, 1H), 8.60 (s, 1H), 8.45 (s, 1H), 8.20 (br, 1H), 7.74 (d, J = 8.2 Hz, 1H), 7.62 (s, 1H), 7.50 (d, J = 8.1 Hz, 1H), 7.45–7.28 (m, 2H), 7.25–7.08 (m, 2H), 6.83–6.65 (m, 1H), 6.56–6.30 (m, 1H), 4.40 (s, 1H), 4.21–4.01 (m, 1H), 3.95 (s, 2H), 3.47–3.19 (m, 2H), 2.80 (s, 6H), 2.13–1.94 (m, 1H), 1.94–1.76 (m, 1H), 1.76–1.41 (m, 2H).

(R,E)-N-(6-(3-((5-chloro-4-(1H-indol-3-yl)pyrimidin-2-yl)amino)piperidine-1-carbonyl)pyridin-3-yl)-4-(dimethylamino)but-2-enamide (10g) LC-MS: *m/z* 559 (M+H). ¹H NMR (500 MHz, DMSO-*d*₆) δ 11.99–11.79 (m, 1H), 10.81–10.54 (m, 1H), 9.88 (s, 1H), 8.92–8.57 (m, 1H), 8.39–8.22 (m, 1H), 8.02 (d, J = 8.6 Hz, 1H), 7.63 (d, J = 8.5 Hz, 1H), 7.55–7.29 (m, 2H), 7.25–7.17 (m, 1H), 7.16–7.05 (m, 2H), 6.91–6.68 (m, 1H), 6.56–6.39 (m, 1H), 3.96 (d, J = 9.2 Hz, 2H), 3.85–3.61 (m, 3H), 3.48 (s, 1H), 3.07 (s, 1H), 2.81 (s, 6H), 2.17–1.94 (m, 2H), 1.84–1.70 (m, 1H), 1.70–1.45 (m, 1H).

(R)-N-(6-(3-((5-chloro-4-(1H-indol-3-yl)pyrimidin-2-yl)amino)piperidine-1-carbonyl)pyridin-3-yl)acrylamide (10h) LC-MS: *m/z* 502 (M+H). ¹H NMR (500 MHz, DMSO-*d*₆) δ 11.80 (s, 1H), 10.66 (s, 1H), 9.78 (s, 1H), 8.98–8.67 (m, 1H), 8.39–8.22 (m, 1H), 8.10 (d, J = 8.6 Hz, 1H), 7.68 (d, J = 8.5 Hz, 1H), 7.55–7.29 (m, 2H), 7.25–7.17 (m, 1H), 7.16–7.05 (m, 2H), 6.85–6.61 (m, 1H), 6.56–6.39 (m, 1H), 4.55 (br, 1H), 3.86 (d, J = 9.0 Hz, 2H), 3.85–3.61 (m, 1H),

Table 6

Mouse Pharmacokinetics of compound BSJ-01-175.

Route	Dose (mg/kg)	T _{max} (h)	C _{max} (ng/mL)	AUC _{last} (h·ng/mL)	T _{1/2} (h)	CL (mL/min/kg)	V _{ss} (L/kg)	F (%)
IV	3		1511	1832	2.2	24.9	3.9	
PO	10	2	272	1043				17

3.48 (s, 1H), 3.07 (s, 1H), 2.27–1.99 (m, 2H), 1.88–1.73 (m, 1H), 1.71–1.45 (m, 1H).

4.1.2. General procedures for synthesis of compound 15a–15h

Substituted 1-fluoro-4-nitrobenzenes or 2-fluoro-5-nitropyridine **11** (1 mmol, 1 equiv) were added to a solution of **5a** (327 mg, 0.7 mmol, 1 equiv) in 3 mL of DMF, followed by addition of 0.1 mL of DIPEA. The resulting mixture was heated to 80 °C and kept stirring for 8 h. The reaction mixture was then cooled to room temperature and the solvent was evaporated to give a brown residue, which was purified by silica gel chromatography column with DCM/methanol (10/1) to afford the desired nitro products **12**. The final compounds 15a–15h were synthesized with similar procedures as **10a–10h**.

(R,E)-N-(4-(3-((5-chloro-4-(1H-indol-3-yl)pyrimidin-2-yl)amino)piperidin-1-yl)phenyl)-4-(dimethylamino)but-2-enamide (15a). LC-MS: *m/z* 530 (M+H). ¹H NMR (500 MHz, DMSO-*d*₆) δ 11.88 (s, 1H), 10.15 (s, 1H), 9.82 (s, 1H), 8.68 (s, 1H), 8.49 (d, *J* = 3.1 Hz, 1H), 8.30 (s, 1H), 7.52 (d, *J* = 8.4 Hz, 2H), 7.48 (d, *J* = 8.2 Hz, 1H), 7.36 (d, *J* = 7.7 Hz, 1H), 7.24–6.86 (m, 4H), 6.74–6.62 (m, 1H), 6.45–6.32 (m, 1H), 3.92 (br, 2H), 3.59 (br, 2H), 2.79 (s, 6H), 2.73–2.62 (m, 1H), 2.04 (br, 1H), 1.88 (br, 1H), 1.72 (br, 1H), 1.55 (br, 1H).

(R)-N-(4-(3-((5-chloro-4-(1H-indol-3-yl)pyrimidin-2-yl)amino)piperidin-1-yl)phenyl)acrylamide (15b). LC-MS: *m/z* 473 (M+H). ¹H NMR (500 MHz, DMSO-*d*₆) δ 11.88 (s, 1H), 10.05 (s, 1H), 8.49 (d, *J* = 3.1 Hz, 1H), 8.30 (s, 1H), 7.57 (s, 2H), 7.48 (d, *J* = 8.2 Hz, 1H), 7.40 (s, 1H), 7.27–6.87 (m, 4H), 6.44–6.32 (m, 1H), 6.27–6.13 (m, 1H), 5.71 (dd, *J* = 10.1, 2.1 Hz, 1H), 4.10 (br, 2H), 3.81 (s, 2H), 2.85 (br, 2H), 2.08 (s, 1H), 1.96–1.85 (m, 1H), 1.77 (br, 1H), 1.58 (br, 1H).

(R,E)-N-(6-(3-((5-chloro-4-(1H-indol-3-yl)pyrimidin-2-yl)amino)piperidin-1-yl)pyridin-3-yl)-4-(dimethylamino)but-2-enamide (15c). LC-MS: *m/z* 531 (M+H). ¹H NMR (500 MHz, DMSO-*d*₆) δ 11.87 (s, 1H), 10.35 (s, 1H), 9.88 (s, 1H), 8.79–8.57 (br, 1H), 8.47 (d, *J* = 3.0 Hz, 1H), 8.38 (s, 1H), 8.31 (s, 1H), 7.83 (s, 1H), 7.54–7.35 (m, 2H), 7.09 (br, 2H), 6.82–6.61 (m, 1H), 6.47–6.32 (m, 1H), 4.32 (br, 1H), 4.10 (br, 1H), 3.95 (dd, *J* = 7.4, 3.3 Hz, 2H), 3.10–2.89 (m, 2H), 2.80 (s, 6H), 2.25–1.95 (m, 1H), 1.87 (s, 1H), 1.72–1.51 (m, 2H).

(R)-N-(6-(3-((5-chloro-4-(1H-indol-3-yl)pyrimidin-2-yl)amino)piperidin-1-yl)pyridin-3-yl)acrylamide (15d). LC-MS: *m/z* 474 (M+H). ¹H NMR (500 MHz, DMSO-*d*₆) δ 11.87 (s, 1H), 10.25 (s, 1H), 8.48 (d, *J* = 3.0 Hz, 1H), 8.39 (br, 2H), 8.32 (s, 1H), 8.04–7.66 (m, 1H), 7.54–7.40 (m, 2H), 7.19 (br, 2H), 6.43–6.32 (m, 1H), 6.30–6.22 (m, 1H), 5.82–5.74 (m, 1H), 4.27 (s, 1H), 4.06 (br, 3H), 3.15–2.99 (m, 2H), 2.05 (br, 1H), 1.91 (br, 1H), 1.74–1.57 (m, 2H).

(R)-N-(4-(3-((5-chloro-4-(1H-indol-3-yl)pyrimidin-2-yl)amino)piperidin-1-yl)-2-methylphenyl)acrylamide (15e). LC-MS: *m/z* 487 (M+H). ¹H NMR (500 MHz, DMSO-*d*₆) δ 11.87 (s, 1H), 9.34 (s, 1H), 8.81–8.61 (br, 1H), 8.49 (d, *J* = 3.1 Hz, 1H), 8.30 (s, 1H), 7.48 (d, *J* = 8.2 Hz, 1H), 7.44–7.07 (m, 3H), 6.92 (br, 2H), 6.55–6.38 (m, 1H), 6.25–6.08 (m, 1H), 5.70 (dd, *J* = 10.1, 2.1 Hz, 1H), 3.86 (br, 2H), 3.55 (br, 1H), 2.97–2.58 (m, 2H), 2.27–1.94 (m, 5H), 1.87 (br, 1H), 1.73 (br, 1H), 1.63–1.36 (m, 1H).

(R)-N-(4-(3-((5-chloro-4-(1H-indol-3-yl)pyrimidin-2-yl)amino)piperidin-1-yl)-3-fluorophenyl)acrylamide (15f). LC-MS: *m/z* 491 (M+H). ¹H NMR (500 MHz, DMSO-*d*₆) δ 11.88 (s, 1H), 10.15 (s, 1H), 8.72 (br, 1H), 8.49 (t, *J* = 8.4 Hz, 1H), 8.29 (s, 1H), 7.66–7.57 (m, 1H), 7.47 (d, *J* = 8.1 Hz, 1H), 7.33 (br, 1H), 7.23 (s, 1H), 7.17 (s, 1H), 7.05 (t, *J* = 9.3 Hz, 1H), 6.93 (s, 1H), 6.43–6.31 (m, 1H), 6.27–6.17 (m, 1H), 5.74 (dd, *J* = 10.1, 2.1 Hz, 1H), 3.51 (br, 2H), 3.32–3.21 (m, 1H), 2.75–2.58 (m, 2H), 2.04 (br, 1H), 1.91–1.80 (m, 1H), 1.74 (br, 1H), 1.60–1.47 (m, 1H).

(R)-N-(4-(3-((5-chloro-4-(1H-indol-3-yl)pyrimidin-2-yl)amino)piperidin-1-yl)-5-fluoro-2-methylphenyl)acrylamide

(15g). LC-MS: *m/z* 505 (M+H). ¹H NMR (500 MHz, DMSO-*d*₆) δ 11.87 (s, 1H), 9.38 (s, 1H), 8.90–8.57 (m, 1H), 8.49 (d, *J* = 3.1 Hz, 1H), 8.28 (s, 1H), 7.47 (d, *J* = 8.1 Hz, 1H), 7.41–7.23 (m, 2H), 7.23–7.07 (m, 1H), 6.92 (d, *J* = 9.4 Hz, 1H), 6.57–6.47 (m, 1H), 6.26–6.17 (m, 1H), 5.77–5.69 (m, 1H), 3.52 (s, 3H), 3.36–3.27 (m, 1H), 2.76–2.58 (m, 2H), 2.19–1.94 (m, 4H), 1.86 (br, 1H), 1.74 (br, 1H), 1.55–1.49 (m, 1H).

(R)-N-(4-(3-((5-chloro-4-(1H-indol-3-yl)pyrimidin-2-yl)amino)piperidin-1-yl)-5-methoxy-2-methylphenyl)acrylamide (15h). LC-MS: *m/z* 517 (M+H). ¹H NMR (500 MHz, DMSO-*d*₆) δ 11.86 (s, 1H), 9.41 (s, 1H), 8.69 (br, 1H), 8.48 (d, *J* = 3.1 Hz, 1H), 8.29 (s, 1H), 7.48 (d, *J* = 8.2 Hz, 1H), 7.31–6.89 (m, 4H), 6.56–6.48 (m, 1H), 6.25–6.18 (m, 1H), 5.76–5.69 (m, 1H), 4.17 (br, 2H), 3.61 (br, 3H), 3.35 (s, 2H), 2.82 (br, 2H), 2.11 (s, 3H), 2.07–1.94 (m, 1H), 1.88 (br, 1H), 1.81 (br, 1H), 1.61 (br, 1H).

4.1.3. General procedures for synthesis of compound 22a–22d

To a suspension of NaH (0.8 g, 8.25 mmol, 2.5 equiv) in 3.0 mL of anhydrous DMF was added 3-aminocyclohexanol HCl salt (0.5 g, 3.3 mmol, 1.0 equiv) slowly at 0 °C and kept stirring for 0.5 h, then substituted 1-fluoro-4-nitrobenzene (3.3 mmol, 1.0 equiv) was added. The reaction mixture was kept stirring at 0 °C for another 30 min, then warm to room temperature and kept stirring for 2 h 1 mL of H₂O was added dropwise to quench the reaction. The mixture was extracted with DCM (100 mL), washed with brine, dried over anhydrous Na₂SO₄, filtered and concentrated under reduced pressure. The residue was purified by silica gel chromatography column to give the desired products **18** as a brown solid. The final compounds 22a–22d were synthesized with similar procedures as **10a–10h**.

(E)-N-(4-(((1R,3R)-3-((5-chloro-4-(1H-indol-3-yl)pyrimidin-2-yl)amino)cyclohexyl)oxy)phenyl)-4-(dimethylamino)but-2-enamide (22a). LC-MS: *m/z* 545 (M+H). ¹H NMR (500 MHz, DMSO-*d*₆) δ 12.12 (br, 1H), 10.92 (s, 1H), 10.38 (s, 1H), 8.71–8.51 (m, 2H), 8.36 (s, 1H), 7.59 (d, *J* = 8.7 Hz, 2H), 7.54 (d, *J* = 8.1 Hz, 1H), 7.34 (d, *J* = 50.9 Hz, 1H), 7.25 (t, *J* = 7.6 Hz, 1H), 7.21–7.13 (m, 2H), 6.95 (d, *J* = 9.0 Hz, 2H), 6.79–6.48 (m, 1H), 6.48 (d, *J* = 15.3 Hz, 1H), 4.81 (br, 1H), 3.89 (t, *J* = 6.1 Hz, 2H), 3.53–3.41 (m, 2H), 2.74 (s, 3H), 2.73 (s, 3H), 2.22–2.10 (m, 1H), 2.02 (br, 1H), 1.88–1.70 (m, 3H), 1.69–1.50 (m, 2H), 1.48–1.33 (m, 1H).

N-(4-(((1R,3R)-3-((5-chloro-4-(1H-indol-3-yl)pyrimidin-2-yl)amino)cyclohexyl)oxy)phenyl)acrylamide (22b). LC-MS: *m/z* 488 (M+H). ¹H NMR (500 MHz, DMSO-*d*₆) δ 11.90 (s, 1H), 10.99 (br, 1H), 10.36 (s, 1H), 8.71 (br, 1H), 8.60 (d, *J* = 8.4 Hz, 2H), 8.36 (br, 1H), 7.66 (d, *J* = 8.7 Hz, 2H), 7.54 (d, *J* = 8.1 Hz, 1H), 7.49–7.31 (m, 1H), 7.25 (t, *J* = 7.6 Hz, 1H), 7.21–7.13 (m, 3H), 7.09–6.96 (m, 2H), 6.62–6.45 (m, 1H), 6.40 (d, *J* = 15.3 Hz, 1H), 5.88 (s, 1H), 4.85 (br, 1H), 3.90 (br, 2H), 3.57–3.45 (m, 2H), 2.22–1.94 (m, 2H), 1.88–1.69 (m, 3H), 1.65–1.52 (m, 2H), 1.46 (br, 1H).

(E)-N-(4-(((1S,3R)-3-((5-chloro-4-(1H-indol-3-yl)pyrimidin-2-yl)amino)cyclohexyl)oxy)phenyl)-4-(dimethylamino)but-2-enamide (22c). LC-MS: *m/z* 545 (M+H). ¹H NMR (500 MHz, DMSO-*d*₆) δ 11.88 (s, 1H), 10.16 (s, 1H), 9.79 (s, 1H), 8.62 (s, 1H), 8.49 (s, 1H), 8.25 (d, *J* = 4.6 Hz, 1H), 7.50 (br, 2H), 7.39–7.26 (m, 1H), 7.25–7.10 (m, 2H), 6.98–6.90 (m, 1H), 6.75–6.62 (m, 1H), 6.41 (d, *J* = 15.3 Hz, 1H), 4.39 (br, 2H), 3.92 (br, 3H), 2.80 (s, 3H), 2.79 (s, 3H), 2.47–2.28 (m, 1H), 2.20–1.94 (m, 2H), 1.79 (br, 1H), 1.55–1.37 (m, 1H), 1.35–1.17 (m, 2H).

(E)-N-(4-(((1R,3R)-3-((5-chloro-4-(1H-indol-3-yl)pyrimidin-2-yl)amino)cyclohexyl)oxy)-3-fluorophenyl)-4-(dimethylamino)but-2-enamide (22d). LC-MS: *m/z* 563 (M+H). ¹H NMR (500 MHz, DMSO-*d*₆) δ 11.86 (s, 1H), 10.37 (s, 1H), 9.80 (s, 1H), 8.66 (d, *J* = 8.0 Hz, 1H), 8.50 (s, 1H), 8.25 (d, *J* = 3.6 Hz, 1H), 7.69 (dd, *J* = 13.3, 2.5 Hz, 1H), 7.48 (d, *J* = 8.1 Hz, 1H), 7.33–7.09 (m, 4H), 6.82–6.66 (m, 1H), 6.49–6.33 (m, 1H), 4.79 (s, 1H), 3.97–3.91 (m, 4H), 2.80 (s, 3H), 2.78 (s, 3H), 2.16 (br, 1H), 1.81 (br, 3H), 1.68–1.48

(m, 2H), 1.48–1.18 (m, 1H).

4.2. Cell lines

TC71 (male) cells were cultured in RPMI + 10% FBS + 1% PSQ. STR genotyping was previously performed to validate cell line identity (Crompton et al., 2014). Jurkat (male), Kelly (male) and Kelly CDK12C1039F were cultured in RPMI media (Gibco, #11875119) containing 10% fetal bovine serum (Gibco, #10437028) and 1% Penicillin/Streptomycin (Thermo Fisher Scientific, #10378016) at 37 °C in 5% CO₂ humidified air. Cell lines were tested negative for mycoplasma contamination (Lonza, #LT07-318).

4.3. Immunoblotting and antibodies

Cells were lysed in RIPA buffer (150 mM NaCl, 1.0% IGEPAL® CA-630, 0.5% sodium deoxycholate, 0.1% SDS, 50 mM Tris, pH 8.0) (Sigma, #R0278) with protease/phosphatase inhibitor cocktail (Roche). The protein concentrations were measured by BCA analysis (Pierce). Equal amounts of protein were resolved by 4–12% Tris-Base gels (Invitrogen), and then transferred to the Immoblot PVDF membrane (BioRad). Proteins were probed with appropriate primary antibodies and IRDye®800-labeled goat anti-rabbit IgG and IRDye®800-labeled goat anti-mouse IgG (LI-COR) secondary antibodies. The membranes were detected on Odyssey CLx system.

Antibodies used in this study include anti-following proteins: Cyclin H (Cell Signaling Technology, #2927S, 1:1000), Cyclin K (Bethyl Laboratories, #A301-939A, 1:1000), *p*-RNA polII Ser2 (Sigma Aldrich, #04-1571-I, 1:1000), *p*-RNA polII Ser5 (Sigma Aldrich, #04-1572-I, 1:1000), *p*-RNA polII Ser7 (Sigma Aldrich, #04-1570-I, 1:1000), RNA PolII (Cell Signaling Technology, #14958S, 1:1000), and β -Actin (Cell Signaling Technology, #3700, 1:1000).

4.4. In vitro kinase assays

The commercial kinase assays from Invitrogen, ADAPTA or Z'LYTE, were chosen to measure the biochemical inhibitory IC₅₀ values for CDK2/CycA, CDK7/CycH, CDK9/CycT1, DNA-PK, RSK2, JNK1, JNK2 and JNK3.

CDK12/13 kinase assay: Radioactive kinase activity measurements were performed using 0.2 mM [³²P]- γ -ATP containing 0.45 mCi [³²P]/mL (PerkinElmer). CDK12/CycK or CDK13/CycK complexes were pre-incubated at 0.2 μ M with varying concentrations of compound for 5 min at 30 °C, followed by addition of substrate and an additional incubation for 15 min at 30 °C. Reactions were stopped by EDTA, added to a final concentration of 50 mM. Mixtures were spotted onto filter sheets of Amersham Protran nitrocellulose membrane (GE Healthcare) and washed three times for 5 min with 0.75% (v/v) phosphoric acid. Radioactivity was counted in a Beckman Liquid Scintillation Counter (Beckman-Coulter) for 1 min.

4.5. Cellular target engagement assays

Cells were lysed in IP lysis buffer (25 mM Tris-HCl pH 7.4, 150 mM NaCl, 1 mM EDTA, 1% NP-40 and 5% glycerol) (Thermo Fisher Scientific, Cat#87788) containing protease/phosphatase inhibitor cocktail (Roche). The protein concentrations were measured by BCA analysis (Pierce). Cell lysates were incubated with 1 μ M biotinylated THZ1 at 4 °C overnight and incubated for 3 more hours at room temperature. Lysates with probe were then incubated with streptavidin beads (Thermo Fisher, #20349) for 2 h at 4 °C. The protein-probe complexes on the beads were then subjected to

immunoblotting as described above.

4.6. Antiproliferation assay

Kelly wild type or CDK12C1039F cells were seeded at the density of 5000 cells/well in 96-well plates and cultured overnight. Compound 22a or THZ531 were then added to cells and incubated for 72 h. Cell viability was determined by using CellTiter-Glo (Promega, #G7571) according to the manufacturer's instructions. IC₅₀ values (defined as the concentration of compound needed to reduce cell viability to 50% of the vehicle DMSO control) were estimated by using GraphPad Prism 8.2.0 (GraphPad Software).

4.7. qRT-PCR

1 μ g of total RNA from cells was reverse transcribed with oligo(dT) and SuperScript IV Reverse Transcriptase (Life Technologies, #18090050). RT-qPCR was performed using a SYBR Green (Life Technologies, #4367659) and the 7500 Fast Real-Time PCR system (Applied Biosystems). All runs were accompanied by the internal control *Gapdh* gene. The samples were run in triplicate and normalized to GAPDH using a $\Delta\Delta$ cycle threshold-based algorithm to provide arbitrary units representing relative expression levels. The primer sequences for specific genes are shown in Table S1.

4.8. Mass spectrometric analysis of recombinant CDK12 protein

CDK12/Cyclin K complex (5 μ g) was treated with DMSO or a 10-fold molar excess of BSJ-01-175 for 1 h at room temperature and analyzed by LC-MS using an HPLC system (Shimadzu, Marlborough, MA) interfaced to an LTQ ion trap mass spectrometer (ThermoFisher Scientific, San Jose, CA). After injection, proteins were desalted for 4 min on column with 100% A, and then eluted with an HPLC gradient (0–100% B in 1 min; A = 0.2 M acetic acid in water; B = 0.2 M acetic acid in acetonitrile). The mass spectrometer was programmed to acquire full scan mass spectra (*m/z* 300–2000) in profile mode (spray voltage = 4.5 kV). Mass spectra were deconvoluted using MagTran software version 1.03b2 [24].

To identify the site of covalent modification, BSJ-01-175 treated CDK12/Cyclin K complex was reduced with 10 mM tris(2-carboxyethyl)phosphine for 10 min at room temperature, alkylated with 20 mM methyl methanethiosulfonate for 10 min at room temperature, and digested with Glu-C protease (Promega, Madison, WI) overnight at 37 °C. Peptides were desalted using C18 (SOLA, ThermoFisher Scientific, Madison, WI), dried by vacuum centrifugation, reconstituted in 50% acetonitrile, 1% formic acid, 100 mM ammonium acetate, and analyzed by CE-MS using a ZipChip CE-MS instrument and autosampler (908 devices, Boston, MA) interfaced to a QExactive HF mass spectrometer (ThermoFisher Scientific). Peptides were resolved at 500 V/cm using an HR chip with a background electrolyte consisting of 50% acetonitrile with 1% formic acid. The mass spectrometer was operated in data dependent mode, and subjected the 5 most abundant ions in each MS scan (*m/z* 300–2000, 60 K resolution, 3E6 target, 100 ms max fill time) to MS/MS (15 K resolution, 1E5 target, 100 ms max fill time). Dynamic exclusion was enabled with a repeat count of 1 and an exclusion duration of 5 s. Raw mass spectrometry data files were converted to.mgf using multiplierz software [25] and searched against a forward-reverse human refseq database using Mascot version 2.6.2. Search parameters specified fixed methylthio modification of cysteine, variable methionine oxidation, and variable BSJ-01-175 modification of cysteine. BSJ-01-175 modified spectra were examined, and figures prepared using mzStudio software. BSJ-01-175 specific product ions were assigned as described [26].

4.9. KiNativ profiling

Kelly cells were plated in fresh media in 15 cm plates and treated for 6 h with DMSO or 1 μ M BSJ-01-175. To harvest cells, plates were washed 3 times with cold PBS, then collected by scraping into 4 mL of cold PBS containing protease and phosphatase inhibitors. Cells were pelleted by centrifugation at 1350g at 4 °C for 5 min and immediately frozen in liquid nitrogen. The frozen samples were sent to ActivX Biosciences (La Jolla, CA) for the remainder of the KiNativ profiling experiment.

4.10. Recombinant proteins

Recombinant human kinases GST-CDK12 (714–1063)/GST-Cyclin K (1–267) and GST-CDK13 (694–1039)/GST-Cyclin K (1–267) were co-expressed with CDK-Activating Kinase (CAK) from *S. cerevisiae* in Sf9 insect cells using the MultiBac^{Turbo} system [27]. Cells expressing the respective kinase complexes were harvested by centrifugation and resuspended in lysis buffer (50 mM Hepes pH 7.4, 300 mM NaCl, 5% glycerol and 5 mM β Me) and disrupted by sonication. The lysate was cleared by centrifugation in a Beckman Avanti J-26S XP centrifuge with a JA-25.50 rotor (20,000 r.p.m. for 45 min at 4 °C) and applied to GSTrap FF columns (GE Healthcare) equilibrated with Lysis buffer using an ÄKTA prime-plus chromatography system (GE Healthcare). Following extensive washes with 10 column volumes (CV) of lysis buffer, the protein was eluted in elution buffer (50 mM Hepes pH 7.4, 300 mM NaCl, 5% glycerol, 5 mM β Me and 10 mM Glutathione).

Proteins were further purified by size exclusion chromatography (SEC) on a Superdex 200 PG column (GE Healthcare) equilibrated in SEC buffer (20 mM Hepes pH 7.4, 150 mM NaCl, 5% glycerol and 1 mM TCEP). Fractions of the main peak containing stoichiometric kinase complexes as determined by SDS–PAGE were pooled and concentrated using Amicon filters (Millipore). Protein was aliquoted, snap frozen in liquid nitrogen and stored at –80 °C.

4.11. Crystallization and structure determination

For crystallization of kinase complexes bound to small molecule inhibitors, proteins were purified as described above. After SEC, compounds were diluted in DMSO, added in a 1:1.5 ratio to the pooled kinase complexes and incubated overnight at 4 °C. Excess free compound was removed by buffer exchange using PD10 desalting column (GE Healthcare). Proteins were concentrated, aliquoted, snap frozen and stored at –80 °C.

The CDK12/CycK protein complex, was stored in a buffer of 20 mM Hepes, pH 7.5, 150 mM NaCl and 1 mM TCEP. Initial needle like crystals were obtained using the hanging drop vapor diffusion technique at 293 K by using the JCSG+ screen (Molecular Dimension). These crystals grew as clusters that showed high mosaicity while testing on the diffractometer and diffracted to about 7 Å resolution. To optimize crystal growth, several techniques were tried, e.g., micro-seeding, streak-seeding and macro-seeding, out of which micro-seeding helped in growing big single crystals by mixing 1 μ l protein solution with 1 μ l of the reservoir solution containing 0.1 M MES, pH 6.0, 30% PEG-mixture (medium weight pegs), 0.3 M NDSB and 0.2 M MgCl₂. Crystallization drops were set up by mixing protein sample and seed stock dilutions in a 1:1 ratio and crystals were grown using the hanging drop vapor diffusion technique at 293 K. Best crystals grew within one week to a size of about approximately 150 \times 40 \times 30 μ m [3] using a 10^{–2} dilution of the seed stock. We harvested many rod-shaped crystals by transferring them into 15% (v/v) ethylene glycol in mother-liquor and flash freezing in liquid nitrogen.

Diffraction data were collected at the Swiss Light Source,

Villigen, at 1.000 Å wavelength and 100 K temperature using the PILATUS 6 M detector. The XDS package was used to process, integrate and scale the data [28]. The structure was solved by molecular replacement using the program PHASER [29] and the coordinates of CDK12/CycK (4NST) as search model. The model was refined by alternate cycles of refinement using PHENIX [30]. The manual rebuilding was made using the graphical program COOT [31]. Molecular diagrams were drawn using PyMOL (<http://www.pymol.org/>).

The purified human CDK13/CycK complex was mixed with THZ531 in molar ratios of 1:5 and incubated on ice for 30 min. Initial micro-crystals were obtained using the hanging drop vapor diffusion technique at 293 K by mixing 1 μ l protein-complex solution with 1 μ l of the reservoir solution of JCSG+ screen containing 0.1 M Bis-Tris (pH 5.5), 25% PEG 3350 and 0.2 M MgCl₂. These conditions were used as template for further refinement to obtain optimal crystals. Final crystallization conditions were set up using the hanging drop vapor diffusion technique at 293 K using 24-well plates (Molecular Dimension). Best crystals grew in about 10 days to a size of about approximately 200 \times 40 \times 30 μ m³ using 0.1 M MES (pH 6.8), 24% PEG 3350 and 0.2 M MgCl₂. For cryo-protection, crystals were transferred to a solution that contained 15% ethylene glycol in mother-liquor. After 5–10 s soaking, crystals were flash-frozen in liquid nitrogen.

Diffraction data were collected at beamline ID23-1 at the European Synchrotron Radiation Facility (ESRF), Grenoble, France, at 0.97242 Å wavelength and 100 K temperature using the PILATUS 6 M detector. Data processing, integration, scaling, molecular replacement and model building was performed as described above. The coordinates of CDK13/CycK (5EFQ) were used as search model.

4.12. Mouse liver microsomal stability

The MLM assays were previously reported and are commercially available from Scripps Florida [32].

4.13. In vivo pharmacokinetic studies

Male Swiss albino mice were dosed with BSJ-01-175 solution formulation (intravenous, 5% NMP, 5% Solutol HS-15, 90% Normal saline, dose 3 mg/kg) or (oral, 5% NMP, 5% Solutol HS-15, 90% Normal saline, dose 10 mg/kg). Blood samples were collected at Pre-dose, 0.08, 0.25, 0.5, 1, 2, 4, 8 and 24 h (IV and IP) and Pre-dose, 0.25, 0.5, 1, 2, 4, 6, 8 and 24 h (PO). The blood samples were collected from sets of three mice at each time point in labeled microcentrifuge tubes containing K2EDTA as an anticoagulant. Plasma samples were separated by centrifugation and stored below –70 °C until bioanalysis. All samples were processed for analysis by precipitation using acetonitrile and analyzed with a partially validated LC/MS/MS method (LLOQ – 1.22 ng/mL for IV and PO, LLOQ – 5.02 ng/mL for IP). Pharmacokinetic parameters were calculated using the noncompartmental analysis tool of WinNonlin Enterprise software (Version 6.3).

4.14. In vivo efficacy studies

In vivo studies were performed at the Dana-Farber Cancer Institute, and all animal protocols were approved by the Dana-Farber Cancer Institute Animal Care and Use Committee. Nude mice were maintained according to institutional guidelines.

Three million TC71 Ewing sarcoma cells were implanted subcutaneously into the right flank of 7–8 weeks old female nude mice. Following engraftment, mice with palpable tumors were divided into two groups and treated with 10 mg/kg BSJ-01-175

(n = 5) or vehicle control (n = 10) administered IP daily. Tumors were measured by caliper twice weekly and weighed. Statistical significance was determined by 2-way ANOVA. BSJ-01-175 was solubilized in the vehicle control, 10% DMSO in D5W, for animal dosing. Treatment holidays were given when mouse weights dropped below 10%.

Author contributions

Conceptualization: N.G., T.Z. M.G.; Chemistry: B.J., F.F.; Biology: J.J., I. K., A. I., K.A., B. S. N.K., K.S. S.D., A.G.; Mass spectrum labeling: S.F., J.M.; Writing: T.Z., M.G., B.J. J.J., N.G.; The manuscript was written through contributions of all authors. All authors have given approval to the final version of the manuscript. ‡These authors contributed equally.

Declaration of competing interest

The authors declare the following financial interests/personal relationships which may be considered as potential competing interests: N.S.G. is a founder, science advisory board member (SAB) and equity holder in Gatekeeper, Syros, Petra, C4, B2S, Aduro and Soltego. The Gray lab receives or has received research funding from Novartis, Takeda, Astellas, Taiho, Janssen, Kinogen, Voronoi, Her2llc, Deerfield, Ephiphanes and Sanofi. N.S.G., T. Z. and B. J. are named inventors on patent applications covering compounds described in this manuscript.

Acknowledgment

We thank Jim Sun at NMR facility of Dana-Farber cancer institute for his assistance on NMR data collection and Milka Kostic for editorial suggestions on the manuscript. We would like to thank the beamline scientists at Swiss Light Source (Villigen, Switzerland) and the European Synchrotron Radiation Facility (Grenoble, France) for access and support. Milka Kostic is greatly acknowledged for the editing and proof reading. M.G. is supported by the Deutsche Forschungsgemeinschaft (GE 976/9-2) under Germany's Excellence Strategy – EXC2151–390873048.

Appendix A. Supplementary data

Supplementary data to this article can be found online at <https://doi.org/10.1016/j.ejmech.2021.113481>.

References

- [1] M. Malumbres, Cyclin-dependent kinases, *Genome Biol.* 15 (6) (2014) 122.
- [2] M. Malumbres, E. Harlow, T. Hunt, T. Hunter, J.M. Lahti, G. Manning, D.O. Morgan, L.H. Tsai, D.J. Wolgemuth, Cyclin-dependent kinases: a family portrait, *Nat. Cell Biol.* 11 (11) (2009) 1275–1276.
- [3] U. Asghar, A.K. Witkiewicz, N.C. Turner, E.S. Knudsen, The history and future of targeting cyclin-dependent kinases in cancer therapy, *Nat. Rev. Drug Discov.* 14 (2) (2015) 130–146.
- [4] C. Bruyere, L. Meijer, Targeting cyclin-dependent kinases in anti-neoplastic therapy, *Curr. Opin. Cell Biol.* 25 (6) (2013) 772–779.
- [5] P. Loyer, J.H. Trembley, R. Katona, V.J. Kidd, J.M. Lahti, Role of CDK/cyclin complexes in transcription and RNA splicing, *Cell. Signal.* 17 (9) (2005) 1033–1051.
- [6] D. Eick, M. Geyer, The RNA polymerase II carboxy-terminal domain (CTD) code, *Chem. Rev.* 113 (11) (2013) 8456–8490.
- [7] B. Bartkowiak, P. Liu, H.P. Phatnani, N.J. Fuda, J.J. Cooper, D.H. Price, K. Adelman, J.T. Lis, A.L. Greenleaf, CDK12 is a transcription elongation-associated CTD kinase, the metazoan ortholog of yeast Ctk1, *Genes Dev.* 24 (20) (2010) 2303–2316.
- [8] E.A. Bowman, W.G. Kelly, RNA polymerase II transcription elongation and Pol II CTD Ser2 phosphorylation: a tail of two kinases, *Nucleus* 5 (3) (2014) 224–236.
- [9] J. Kohoutek, D. Blazek, Cyclin K goes with Cdk12 and Cdk13, *Cell Div.* 7 (2012) 12.

- [10] K. Liang, X. Gao, J.M. Gilmore, L. Florens, M.P. Washburn, E. Smith, A. Shilatifard, Characterization of human cyclin-dependent kinase 12 (CDK12) and CDK13 complexes in C-terminal domain phosphorylation, gene transcription, and RNA processing, *Mol. Cell Biol.* 35 (6) (2015) 928–938.
- [11] I. Bajrami, J.R. Frankum, A. Konde, R.E. Miller, F.L. Rehman, R. Brough, J. Campbell, D. Sims, R. Rafiq, S. Hooper, L. Chen, I. Kozarewa, I. Assiotis, K. Fenwick, R. Natrajan, C.J. Lord, A. Ashworth, Genome-wide profiling of genetic synthetic lethality identifies CDK12 as a novel determinant of PARP1/2 inhibitor sensitivity, *Canc. Res.* 74 (1) (2014) 287–297.
- [12] D. Blazek, J. Kohoutek, K. Bartholomeeusens, E. Johansen, P. Hulinkova, Z. Luo, P. Cimermancic, J. Ule, B.M. Peterlin, The Cyclin K/Cdk12 complex maintains genomic stability via regulation of expression of DNA damage response genes, *Genes Dev.* 25 (20) (2011) 2158–2172.
- [13] S.J. Dubbury, P.L. Boutz, P.A. Sharp, CDK12 regulates DNA repair genes by suppressing intronic polyadenylation, *Nature* 564 (7734) (2018) 141–145.
- [14] K.M. Ekumi, H. Paculova, T. Lenasi, V. Pospichalova, C.A. Bosken, J. Rybarikova, V. Bryja, M. Geyer, D. Blazek, M. Barboric, Ovarian carcinoma CDK12 mutations misregulate expression of DNA repair genes via deficient formation and function of the Cdk12/CycK complex, *Nucleic Acids Res.* 43 (5) (2015) 2575–2589.
- [15] M. Krajewska, R. Dries, A.V. Grasseti, S. Dust, Y. Gao, H. Huang, B. Sharma, D.S. Day, N. Kwiatkowski, M. Pomaville, O. Dodd, E. Chipumuro, T. Zhang, A.L. Greenleaf, G.C. Yuan, N.S. Gray, R.A. Young, M. Geyer, S.A. Gerber, R.E. George, CDK12 loss in cancer cells affects DNA damage response genes through premature cleavage and polyadenylation, *Nat. Commun.* 10 (1) (2019) 1757.
- [16] S.F. Johnson, C. Cruz, A.K. Greifenberg, S. Dust, D.G. Stover, D. Chi, B. Primack, S. Cao, A.J. Bernhardt, R. Coulson, J.B. Lazaro, B. Kochupurakkal, H. Sun, C. Unitt, L.A. Moreau, K.A. Sarosiek, M. Scaltriti, D. Juric, J. Baselga, A.L. Richardson, S.J. Rodig, A.D. D'Andrea, J. Balmana, N. Johnson, M. Geyer, V. Serra, E. Lim, G.I. Shapiro, CDK12 inhibition reverses De Novo and acquired PARP inhibitor resistance in BRCA wild-type and mutated models of triple-negative breast cancer, *Cell Rep.* 17 (9) (2016) 2367–2381.
- [17] A.B. Iniguez, B. Stolte, E.J. Wang, A.S. Conway, G. Alexe, N.V. Dharra, N. Kwiatkowski, T. Zhang, B.J. Abraham, J. Mora, P. Kalev, A. Leggett, D. Chowdhury, C.H. Benes, R.A. Young, N.S. Gray, K. Stegmaier, EWS/FLI confers tumor cell synthetic lethality to CDK12 inhibition in Ewing sarcoma, *Canc. Cell* 33 (2) (2018) 202–216 e6.
- [18] T. Zhang, N. Kwiatkowski, C.M. Olson, S.E. Dixon-Clarke, B.J. Abraham, A.K. Greifenberg, S.B. Ficarro, J.M. Elkins, Y. Liang, N.M. Hannett, T. Manz, M. Hao, B. Bartkowiak, A.L. Greenleaf, J.A. Marto, M. Geyer, A.N. Bullock, R.A. Young, N.S. Gray, Covalent targeting of remote cysteine residues to develop CDK12 and CDK13 inhibitors, *Nat. Chem. Biol.* 12 (10) (2016) 876–884.
- [19] N. Kwiatkowski, T. Zhang, P.B. Rahl, B.J. Abraham, J. Reddy, S.B. Ficarro, A. Dastur, A. Amzallag, S. Ramaswamy, B. Tesar, C.E. Jenkins, N.M. Hannett, D. McMillin, T. Sanda, T. Sim, N.D. Kim, T. Look, C.S. Mitsiades, A.P. Weng, J.R. Brown, C.H. Benes, J.A. Marto, R.A. Young, N.S. Gray, Targeting transcription regulation in cancer with a covalent CDK7 inhibitor, *Nature* 511 (7511) (2014) 616–620.
- [20] C.A. Bosken, L. Farnung, C. Hintermair, M. Merzel Schachter, K. Vogel-Bachmayr, D. Blazek, K. Anand, R.P. Fisher, D. Eick, M. Geyer, The structure and substrate specificity of human Cdk12/Cyclin K, *Nat. Commun.* 5 (2014) 3505.
- [21] A.K. Greifenberg, D. Honig, K. Pilarova, R. Duster, K. Bartholomeeusens, C.A. Bosken, K. Anand, D. Blazek, M. Geyer, Structural and functional analysis of the Cdk13/cyclin K complex, *Cell Rep.* 14 (2) (2016) 320–331.
- [22] M.P. Patricelli, T.K. Nomanbhoy, J. Wu, H. Brown, D. Zhou, J. Zhang, S. Jagannathan, A. Aban, E. Okerberg, C. Herring, B. Nordin, H. Weissig, Q. Yang, J.D. Lee, N.S. Gray, J.W. Kozarich, In situ kinase profiling reveals functionally relevant properties of native kinases, *Chem. Biol.* 18 (6) (2011) 699–710.
- [23] Y. Gao, T. Zhang, H. Terai, S.B. Ficarro, N. Kwiatkowski, M.F. Hao, B. Sharma, C.L. Christensen, E. Chipumuro, K.K. Wong, J.A. Marto, P.S. Hammerman, N.S. Gray, R.E. George, Overcoming resistance to the THZ series of covalent transcriptional CDK inhibitors, *Cell. Chem. Biol.* 25 (2) (2018) 135–142, e5.
- [24] Z. Zhang, A.G. Marshall, A universal algorithm for fast and automated charge state deconvolution of electrospray mass-to-charge ratio spectra, *J. Am. Soc. Mass Spectrom.* 9 (3) (1998) 225–233.
- [25] W.M. Alexander, S.B. Ficarro, G. Adelman, J.A. Marto, Multiplierz v2.0: a Python-based ecosystem for shared access and analysis of native mass spectrometry data, *Proteomics* 17 (15–16) (2017).
- [26] S.B. Ficarro, C.M. Browne, J.D. Card, W.M. Alexander, T. Zhang, E. Park, R. McNally, S. Dhe-Paganon, H.S. Seo, I. Lamberto, M.J. Eck, S.J. Buhrlage, N.S. Gray, J.A. Marto, Leveraging gas-phase fragmentation pathways for improved identification and selective detection of targets modified by covalent probes, *Anal. Chem.* 88 (24) (2016) 12248–12254.
- [27] C. Bieniossek, T. Imasaki, Y. Takagi, I. Berger, MultiBac: expanding the research toolbox for multiprotein complexes, *Trends Biochem. Sci.* 37 (2) (2012) 49–57.
- [28] W. Kabsch, Xds, *Acta Crystallogr. D Biol. Crystallogr.* 66 (Pt 2) (2010) 125–132.
- [29] A.J. McCoy, R.W. Grosse-Kunstleve, P.D. Adams, M.D. Winn, L.C. Storoni, R.J. Read, Phaser crystallographic software, *J. Appl. Crystallogr.* 40 (Pt 4) (2007) 658–674.
- [30] P.D. Adams, P.V. Afonine, G. Bunkoczi, V.B. Chen, I.W. Davis, N. Echols, J.J. Headd, L.W. Hung, G.J. Kapral, R.W. Grosse-Kunstleve, A.J. McCoy, N.W. Moriarty, R. Oeffner, R.J. Read, D.C. Richardson, J.S. Richardson,

- T.C. Terwilliger, P.H. Zwart, PHENIX: a comprehensive Python-based system for macromolecular structure solution, *Acta Crystallogr. D Biol. Crystallogr.* 66 (Pt 2) (2010) 213–221.
- [31] P. Emsley, K. Cowtan, Coot: model-building tools for molecular graphics, *Acta Crystallogr. D Biol. Crystallogr.* 60 (Pt 12 Pt 1) (2004) 2126–2132.
- [32] X. Li, Y. He, C.H. Ruiz, M. Koenig, M.D. Cameron, T. Vojtkovsky, Characterization of dasatinib and its structural analogs as CYP3A4 mechanism-based inactivators and the proposed bioactivation pathways, *Drug Metab. Dispos.* 37 (6) (2009) 1242–1250.